High-resolution throw-depth mapping to assess the evolution and reactivation histories of outer-arc faults in buckle folds

Abubakar Maunde[a, b], Tiago M. Alves[a,*]

[a] 3D Seismic Lab, School of Earth and Environmental Sciences, Cardiff University, United Kingdom

[b] Department of Applied Geophysics, Faculty of Physical Sciences, Modibbo Adama University, Yola, Nigeria

***Corresponding author**: E-mail: abubakarmaunde@mau.edu.ng

Abstract

Tectonic shortening can induce a continuum of internal deformation in strata and leads to the generation of outer-arc extensional faults in evolving folds and structural traps. High-quality three-dimensional (3D) seismic and borehole data from the Southern North Sea are used in this work to investigate the geometry and growth histories of outer-arc extensional faults via a detailed analysis of fault throws vs. their depths (T-z plots). The results show that faults nucleated first in more competent sandy intervals - those recording the larger fault throws between 21.3 m and 41.1 m, and a high competency ratio above 1.0. They propagated outwards to link with fault segments developing in less competent shale-rich intervals. These softer shaley intervals record fault throws between 5.2 m and 19.6 m and competency ratios below 1.0. Throw-depth distributions suggest fault growth via segment linkage whereby the segments with the larger throws propagate outwards towards each other to then link to strata recording small fault throws. Fault traces are also narrower, more localised and less segmented compared to incompetent shale-rich intervals. Recognising the geometry and growth histories of outer-arc extensional faults as those in this work is crucial to understanding how faults evolve and grow near folds and horizontally shortened traps. It also provides information on the timing of fault activity, a parameter directly affecting sub-surface fluid flow and the sealing potential

of faults in geological reservoirs. As a corollary, we show that the loci where outer-arc faults first nucleated and subsequently propagated from is recorded by anomalous fault-throw distributions.

Keywords: 3D seismic data; horizontal shortening; outer-arc normal fault; fault throw segmentation; mechanical stratigraphy; seismic resolution.

1. Introduction

Outcrop geological information, seismic data, and numerical models are frequently used to investigate the geometry and growth history of tectonic faults (Peacock and Sanderson, 1991; Cowie and Scholz, 1992; Kim et al., 2000; Cartwright et al., 1995; Kim and Sanderson, 2005; Maunde et al., 2021). These methods have shown that faults grow as isolated structures in their early stages, with their subsequent propagation continuing via soft linkages between different fault segments to, finally, develop hard-linked strands (Cartwright et al., 1995; Mansfield and Cartwright, 2001; Peacock and Sanderson, 1991; Dawers and Anders, 1995; Lohr et al., 2008). In the published literature, this has led to the well-established concepts of 'linked' or 'coherent' faults, which contrast to the 'isolated' fault growth models that are typical of discrete faults that do not interact in time and space (Barnett et al., 1987; Walsh and Watterson, 1988; Walsh et al., 2002).

Notwithstanding the above concepts, it is hard to discriminate between fault growth models in practical terms, as linked or coherent faults are commonly part of a larger zone of deformation that includes discrete, 'isolated' structures (Nicol et al., 2005). Also, the continuous, progressive process under which faults grow in the three-dimensional space results in the formation of large-scale fault traces via segment linkage for both 'coherent' and 'isolated' structures, a character that results in the overprinting of geological and structural data from the 'isolated' phases of fault growth (Mansfield and Cartwright, 2001; Cartwright et al., 1995; Dawers and Anders, 1995). Compounding this problem, a great part of the published fault-growth models are based on the analysis of large, tectonic faults that are well documented in seismic data and outcrop but are linked to (i.e. grew from) pre-existing basement structures, which are a major control on fault propagation. In parallel, faults that propagate through mechanically layered rock sequences commonly show changes in dip that are visible in cross-section, with steeper fault segments occurring in competent intervals (e.g., limestones, quartzites and sandstones) and gently dipping fault segments being more common in softer intervals (e.g., shales, clays and muds) (Peacock 2002; Roche et al. 2012; Ferrill et al. 2017). Such changes in dip along a fault segment can locally cause the refraction of fault trajectories as the fault propagates through mechanically layered strata - slip along gently dipping fault segments in the less competent strata intervals is accompanied by the dilation (enlargement) of steep fault segments in the competent intervals (Peacock and Sanderson 1991; Ferrill et al. 2017). The resulting dilated (steep) segments of refracted faults and fractures can potentially enhance fluid migration.

This work aims at characterising the geometry and growth histories of outer-arc extensional faults through the detail mapping of fault geometry and throw distributions using high-resolution seismic and borehole data from the Broad Fourteens Basin, Southern North Sea (Fig. 1). The availability of such seismic data means that individual faults could be mapped, and the geometries and growth histories of 258 fault traces quantified in detail. This information was used to determine the way fault traces vary through time, and how their geometries relate to the sedimentary successions that interact with growing faults. In contrast with the published literature, the faults investigated in this article are not rooted in basement units, so the factors controlling their growth are not controlled by any pre-existent structural inheritance. The investigated faults comprise normal dip-slip systems of outer-arc extensional faults that resulted from tectonic buckling (horizontal shortening) of Cretaceous stratigraphic units. In summary, this article aims to address the following research questions:

a) What fault geometries are associated with the horizontal shortening of outer-arc regions of folds?
b) What mode(s) of fault growth are associated with the progressive folding of buried successions?
c) What are the mechanical controls on fault propagation in outer-arc regions of folds?

The approach in this work is important because horizontal shortening has an impact on the architecture of sub-surface reservoirs and their compartmentalisation styles; tectonic movements reactivate faults to allow the secondary migration of fluids into shallower strata (Ward et al., 2016; Bentham et al., 2013; Cartwright et al., 2007). To understand how tectonic shortening impacted, and still controls, the geometry and growth style of pre-existing fault systems, is crucial when evaluating fault zone architecture in folds and structural traps (McClay, 1990; Caine et al. 1996; Ward et al., 2016).

2. Tectono-stratigraphic setting of the Broad Fourteens Basin

The geodynamic evolution of the Broad Fourteens Basin (BFB) was controlled by three (3) tectonic phases: 1) Pre-rift/rift onset phases (Palaeozoic), 2) Syn-rift phase (Mesozoic), and 3) Inversion phase (Late Cretaceous-Cenozoic) (Fig. 2).

2.1 Pre- and rift-onset phases

During the pre-rift/rift onset phase, thick lacustrine and deltaic intervals with interbedded coal seams were deposited as part of the Limburg Group (Gerling et al., 1999; Van Wijhe, 1987) (Fig. 2). Upper Rotliegend terrestrial sandstones were deposited above the so-called Saalian unconformity and became the major reservoir for Permian gas plays offshore the Netherlands (Van Wees et al., 2000; Van Verweij and Simmelink, 2002). The Zechstein Sea subsequently flooded the study area in the Latest Permian. Carbonate-evaporite cycles in Zechstein evaporites reflect fluctuations in sea level, but thick deposits of Zechstein evaporites were still deposited in the northern part of the BFB to form effective seal units for Permian gas plays (Coward, 1995) (Figs. 2 and 3).

2.2 Mesozoic syn-rift phase

Rifting was intensified during the Early Triassic, leading to important differential subsidence in the Southern North Sea (Alves and Elliott, 2014; Duin et al., 2006). Aeolian sands and lacustrine claystones from the Lower and Upper Germanic Trias Group were deposited in the rapidly subsiding BFB at this time. Towards the end of the Triassic, salt tectonics and reactive diapirism occurred along extensional boundary faults near which tectonic movements were localised (Stewart and Coward, 1995; Ziegler, 1992; Van Hulten, 2010). Rift-raft tectonics during the Jurassic led to the further deepening of the BFB and consequent establishment of open marine conditions (Alves and Elliott, 2014; Penge et al., 1996). The deep-water Altena Group was thus deposited in the BFB, with the more bituminous Posidonia Shale Formation comprising the source interval for Jurassic oil plays in the basin (Van Wijhe, 1987; Van Verweij and Simmelink, 2002; Duin et al., 2006) (Fig. 2).

A major sea-level highstand accompanied post-rift subsidence in the BFB and led to the accumulation of thick layers of chalk during the Cretaceous (Van Wijhe, 1987; Van Verweij and Simmelink, 2002).

2.3 Inversion phase

In the Late Cretaceous, N-S Alpine compression interrupted the hitherto predominant tectonic subsidence, with Sub-hercynean inversion reactivating Variscan faults with a reverse-dextral motion (De Lugt et al., 2003; Nalpas et al., 1995). An erosional maximum (~3000 m) took place in the centre of the inverted BFB, at the axis of tectonic inversion (Nalpas et al., 1995; De Lugt et al., 2003). Three additional inversion episodes grouped as the Laramide, Pyrenean and Savian phases took place in the BFB, and were themselves separated by periods of subsidence.

The Laramide inversion reactivated Sub-hercynean faults in the Cenozoic, creating a prominent Cretaceous-Tertiary unconformity (Oudmayer and De Jager, 1993; De Lugt et al., 2003). Other basin inversion events were subsequently recorded in the Cenozoic, the largest of which coincided with the

Pyrenean Orogeny (Oligocene) and created an unconformity at the base of the Miocene (Oudmayer and De Jager, 1993; Van Verweij and Simmelink, 2002). It separates the Lower North Sea Group from the Middle North Sea Group (Wong et al., 2001). The boundary between the Middle and Upper North Sea Groups is marked by the Middle Miocene Savian unconformity (Oudmayer and De Jager, 1993; Wong et al., 2001). In summary, the interval of interest to this study spans Upper Mesozoic to Lower Cenozoic strata, and was intersected by fault systems, first formed in the Upper Cretaceous, that were very mildly reactivated in the Lower Cenozoic (Fig. 2).

3. Data and methods

3.1. Seismic data

The 3D seismic volume used in this work covers an area of 845 km^2 at a water depth of c. 38 m (Fig. 1). The seismic data were zero-phase pre-stack time migrated and processes at a 2-millisecond sampling interval, and a 25 x 25 m bin size. The vertical scale of the seismic data is in TWTT, and its recording length is about 3.5 seconds (Fig. 3).

The high quality of the interpreted 3D seismic volume permitted a detailed visualisation and mapping of fault geometries and throw distributions (Figs. 3 to 4). Hence, interval velocities for strata crossed by wells K15-01 and K15-04 were used in our depth and thicknesses estimates of the interpreted seismic units (Table 1). Based on the observed range of interval velocities – between 2185 m/s and 2856 m/s - and the dominant frequency content of the seismic data (40 Hz), the vertical resolution of the seismic data was estimated to be 13.5 m in the shallow Cretaceous to Cenozoic strata, and c. 17 m in Upper Palaeozoic and Mesozoic strata (Figs. 3 and 4). The relatively high resolution of the seismic data allowed the mapping of seismic horizons and fault traces in detail (Figs. 3 and 4).

3.2. Methods

3.2.1 Seismic interpretation

Seismic horizons and fault traces were identified and mapped using the Petrel® seismic interpretation software. Seven (7) seismic units - S1 to S7 - were mapped and correlated with stratigraphic information from Penge et al. (1999) and van Verweij and Simmelink (2002) (Fig. 2). These seismic units include Unit S1 (Rotliegend and Limburg Groups), Unit S2 (Zechstein Salt), Unit S3 (Germanic Group), Unit S4 (Altena Group), Unit S5 (Rijnland and Schieland Groups), Unit S6 (Chalk Group), and the shallower Unit S7 (North Sea Group) (Fig. 2; Table 1).

Unit S5 is the main target of interest as this unit is intersected by outer-arc faults. Moreover, the unit comprise reservoir intervals inside which oil derived from the Posidonia Shale Formation (Unit S4) is stored (Van Wijhe, 1987; Van Verweij and Simmelink, 2002; Duin et al., 2006) (Fig. 2).

We sub-divided Unit S5 into three (3) seismic sub-units, S5a, S5b and S5c, to further classify them into competent and incompetent intervals based on their lithologies and competency ratios. The data required for such a classification were taken from wells K15-01 and K15-04 (Table 2).

3.2.2 Definition of competency ratios

In this paper, competent units are sand-rich dominant lithologies with a relatively high interval velocity (Vp) and a competency ratio (C) greater than one (> 1). Softer, incompetent units are shale-rich, present a relatively low interval velocity (Vp), and a competency ratio (C) of less than one (< 1). Rock competency (C) is expressed as the ratio of a unit's interval velocity ($V\alpha$) to the adjacent unit's interval velocity ($V\gamma$) (Equation 1):

$$C = \frac{V\alpha}{V\gamma} \quad \text{(Eq. 1)}$$

This ratio assumes that interval velocity is the function of lithology (mineral and texture), density (strength and stiffness), fluid content, porosity, shear and bulk modulus, which are the primary variables that define the mechanical behaviour of an interval (Castagna et al., 1985 and Keary and Brooks 1991). Thus, as proxy, the mechanical behaviour of a rock unit is related to Vp and expressed by Equation 2 as:

$$Vp = \sqrt{\frac{K + \frac{4}{3}\mu}{\rho}} \quad \text{(Eq. 2)}$$

where C is the rock competency ratio, $V\alpha$ and $V\gamma$ are rock unit interval velocity and adjacent rock unit interval velocity, respectively. In Equation 2, K is the bulk modulus (the inverse of compressibility), μ is the shear modulus (rigidity) and ρ is the density of the studied interval. Uncertainties associated with the estimated velocity-derived competency may arise either by increasing or decreasing the position in depth of the recorded sonic log readings. Errors associated with spurious sonic log estimates may also affect the interval velocity values and competency ratio. These limitations will affect the absolute value of estimated interval velocity and competency ratio.

Faults that intersect competent and incompetent units were mapped to assess their geometry and reactivation history. To this mapping was added fault-throw vs. depth (T-z) data at regular intervals of 2-4 ms along their planes (Figs. 5 to 10). Fault throw vs. distance (T-x) data were also acquired along fault traces at a short distance of 12.5 m (Figs. 9 and 10). Keeping a consistently high sampling density was important for recognising the minimum and subtle local fault throw distribution patterns as demonstrated in Tao and Alves (2019) and Alves et al. (2025). Throw data for the interpreted faults were acquired by measuring the differences between footwall and hanging-wall horizon cut-offs. These measurements were taken along the fault planes on seismic profiles perpendicular, and oblique, to local fault strike, bearing in mind local changes in fault geometry and strike. Therefore, fault throw (T) data were thus plotted against depth (z) and contoured to evaluate structural information on multiple parameters such as fault nucleation, fault segmentation, reactivation history and rock competence.

Measurement of fault-throw values depend on the vertical sampling interval of the seismic data, rather than the vertical seismic resolution (Tao and Alves, 2017). The sampling interval of the seismic dataset is 2 ms, and the minimum fault offset resolved on-screen during fault-throw analysis varies from 2 ms (1.9 m) to 3 ms (3.8 m). Therefore, the sampling interval is the key factor in measuring fault-throws rather than the vertical seismic resolution. Uncertainties associated with the measurement of fault-throw values may arise from the vertical sampling rate, the positions of strata terminations and velocity estimates. Nevertheless, the technique used in this paper to quantify the differences in rock competency and fault throw is robust considering the high resolution (and quality) of the seismic volume (Figs. 3 to 6).

4. Interpreted seismic units

Seven (7) seismic units including, Units S1 to S7 were mapped and correlated with stratigraphic data from Penge et al. (1999) and van Verweij and Simmelink (2002) (Fig. 2). These seismic units were grouped under the three (3) main tectonic phases affecting the Broad Fourteens Basin, offshore the Netherlands (Fig. 2; Table 1).

4.1 Pre-rift/rift onset tectonic phase (Upper Palaeozoic)

Units S1 and S2 were deposited during the pre-rift/rift onset phase and are Carboniferous to Late Permian in age (Fig. 2; Table 1).

4.1.1 Unit S1 (Carboniferous to middle Permian)

Unit S1 correlates with the Limburg and Rotliegend groups (Figs. 2 and 3). This unit is characterised by its moderate frequency and faulted low-amplitude seismic reflections (Figs. 3 and 4). Its strata reach a thickness of 1642 m and a p-wave velocity (Vp) of 2856 m/s (Table 1). The lower part of Unit S1 comprises deltaic and lacustrine intervals that are part of the Limburg Group. Interbedded coal seams are part of the Westphalian Coal Measures, a key source of gas in the North Sea (Gerling et al., 1999; Van Wijhe, 1987) (Fig. 2). The upper part of Unit S1 belongs to the Rotliegend Group and comprises terrestrial sandstones of the Slochteren Formation, a major reservoir interval for gas in the study area (Verweij and Simmelink, 2002) (Fig. 2).

Unit S1 is bounded at its top by a thick Zechstein salt layer (Unit S2), which provides an effective seal rock for Permian gas plays (Coward, 1995).

4.1.2 Unit S2 (Late Permian)

Unit S2 comprises a main salt unit and belongs to the Zechstein group (Penge et al., 1999; van Verweij and Simmelink, 2002) (Fig. 2). The unit is characterised by its chaotic, low-amplitude internal seismic reflections. It shows an average Vp of 4203 m/s and a thickness reaching 840 m (Figs. 4 and 5; Table 1). On the interpreted seismic sections, a high-amplitude faulted seismic reflector separates the lower boundary of this unit from Upper Rotliegend sandstones. Its upper boundary is characterised by continuous high-amplitude seismic reflections (Figs. 3 and 4). Large listric faults were rooted in, or instead detached, on top of this unit. In the Southern North Sea, Unit S2 provides an effective seal rock for Permian gas plays (Coward, 1995).

4.2 Syn-rift tectonic phase (Mesozoic)

The syn-rift tectonic phase is materialised in the study area by Units S3, S4 and S5, which span from the Early Triassic to the Early Cretaceous in age (Fig. 2).

4.2.1 Unit S3 (Early to Late Triassic)

Unit S3 correlates with the Germanic Trias Group and comprises sandstones, carbonates, siltstones, and claystones (Penge et al., 1999). In seismic data, Unit S3 forms a package of moderate amplitude and moderate-to-high frequency seismic reflections. It has an average Vp of 2745 m/s and a thickness of 618 m (Figs. 3 and 4; Table 1). The unit is conformable above the bright reflections that mark the top of Unit S2 (Zechstein salt; Van Hulten, 2010). Sandstones and claystones of the Buntsandstein Formation (i.e. lower part of Unit S3) are prolific gas reservoirs, mainly where evaporites in Unit S2 have been withdrawn and salt welds were formed between Units S3 and S1 (Van Hulten, 2010).

4.*2.2 Unit S4 (Late Triassic to Middle Jurassic*)

Unit S4 correlates with the Altena Group and comprises argillaceous deposits, some calcareous intercalations, and thicker carbonate and clastic intervals. In seismic data, Unit S4 forms a package of high-amplitude, high-frequency seismic reflections with an average Vp of 2067 m/s and a thickness reaching 517 m (Figs. 3 and 4; Table. 1). The more bituminous Posidonia Shale Formation is the main source rock for oil in the Southern North Sea (van Verweij and Simmelink, 2002; Duin et al., 2006).

4.2.3 Unit S5 (Late Jurassic to Early Cretaceous)

Unit S5 correlates with the Rijnland Group and comprises coarse clastic intervals, carbonaceous claystones, and interbedded sandstones (van Verweij and Simme link, 2002; Van Adrichem Boogaert and Kouwe, 1993) (Fig. 2). In seismic data, this unit forms a package of high-amplitude, high-frequency seismic reflections and deformed locally by closely spaced normal faults (Figs. 3 and 5). It has an average Vp of 2436 m/s and a thickness of c. 1038 m (Table 1).

In this study, Unit S5 is the main interval of interest, as is deformed by outer-arc faults. It also comprises the reservoir intervals from which oil are sourced from the Posidonia Shale Formation (Unit S4) (Van Wijhe, 1987; Van Verweij and Simmelink, 2002; Duin et al., 2006) (Fig. 2).

4.3 Tectonic-inversion phase (Late Mesozoic to Cenozoic)

4.3.1 Unit S6 (Late Cretaceous)

Unit S6 correlates with the Chalk Group and comprise limestones, marls, calcareous claystones, and glauconitic sands (van Verweij and Simmelink, 2002). Unit 6 has Vp values of c. 3907 m/s, and a thickness around 879 m (Fig. 3; Table 1). It is bounded at its top by the Base Tertiary Unconformity (horizon H6), marking the level at which an erosion maximum took place (Figs. 3, 4 and 5).

The overall thickness of this unit changes significantly, especially where maximum erosion occurred at its top (Fig. 3). The unit is characterised by chaotic internal reflections, in places with low amplitude and high frequency.

4.3.2 Unit S7 (Paleocene to Recent)

Unit S7 correlates with the North Sea Group, which comprises sandstones, clays, silts, locally gravel or peat and brown coal seams (van Verweij and Simmelink, 2002; Van Adrichem Boogaert and Kouwe, 1993). In seismic data, Unit S7 form a package of high-frequency, continuous and moderate to high-amplitude seismic reflections, with an interval velocity (Vp) of 2185 m /s and a thickness of c. 678 m (Figs. 3 and 5; Table. 1). The unit overlies the Chalk Group (Unit S6) and is bounded at its top by the seafloor (Figs. 2 and 4). Where maximum erosion took place, the unit directly overlies Unit 5 (Fig. 4).

5. Outer-arc faults

The fault systems investigated in this work are associated with horizontal shortening (buckling) of overburden rocks, with a moderate horizontal shortening of c. 24% being recorded in the study area (Figs. 3, 5 and 6).

5.1 Geometry of outer-arc faults

In the BFB, seismic data image closely spaced sets of normal faults that are localised in the hinge region of a broad anticline (Fig. 5). These faults are continuous and segmented, offsetting overburden strata around the hinge region of a broad anticline, with some of the upper tips eroded at horizon H6

(Fig. 5). However, some of these eroded faults appear to have been reactivated and mildly propagated upwards into Cenozoic strata (Fig. 6).

Outer-arc normal fault systems in the BFB primarily result from the progressive buckling and folding of upper Mesozoic units in response to the tectonic shortening affecting the Southern North Sea in the Late Cretaceous, and accommodated a significant part of the buckling-related strain occurring in the hinge zone of a broad anticline (Figs. 3 and 6). They are laterally continuous, less segmented and linked over the main NW-SE trending anticline (Fig. 7). The faults have trace lengths of 2200–1100 m, spacings of 550-3000 m and throws between 2 ms and 28 ms (Figs. 7 and 8).

Figures 7 and 8 also highlight the plan-view geometric expression of the interpreted faults through competent sand-rich and incompetent shale-rich intervals, when the fault trace sections in the competent sand-rich intervals (Unit S5c) are compared to fault trace sections in the incompetent shale-rich intervals (Unit S5a), notable changes in fault traces geometries are observed. In the competent sand-rich intervals (Unit S5c), the fault traces are closely spaced and more localised with narrower deformational zones (Fig. 7b). In contrast, incompetent shale-rich intervals (Unit S5a) have fault traces are widely spaced and less localised (Fig. 8b).

5.2 Outer-arc fault throw distribution

Seismic data show that the study area is characterised by keystone normal faults and deeply rooted listric faults (Figs. 3 to 6). Keystone faults *sensu* Rowan et al. (1999) comprise closely spaced normal faults that resulted from buckling and outer-arc stretching of strata during Late Cretaceous to Paleogene tectonic inversion (Maunde and Alves, 2022) (Figs. 3 and 5). These faults predominantly offset the Jurassic to Cretaceous strata (Units S4 and S5), with most of them terminating at the base of Tertiary boundary (H6). Outer-arc faults are dominantly characterised by a curvilinear-polygonal pattern that strikes in a NW-SE direction, i.e. parallel to the longitudinal axis of the BFB (Figs. 4, 8 and 9).

The modes of propagation and growth of the interpreted outer-arc extensional faults were investigated using the geometry and distribution of representative fault throw in Figs. 9 and 10. These faults are characterised by an anomalous distributions of throw along their fault planes, with multiple throw maxima (A) separated by localised throw minima (B) (Figs. 9 and 10). Segments or zones with local throw maxima (A) indicate the intervals where faults were first nucleated at depth, whereas segments or zones with local throw minima (B) relate to the intervals in which pre-existing faults with local throw maxima (A) linked together. They mark the linkage points of pre-existing faults with larger throws (A). Thus, these anomalous faults throw distributions indicate mode of fault growing via segment linkage, as multiple segments, or zones of local throw maxima (A) are separated by segments or zones of local throw minima (B) (e.g., Maunde and Alves, 2020; Baudon and Cartwright, 2008) (Figs. 9 and 10).

An important aspect is that the gamma-ray curves and seismic data in this figure show that Faults F1 and F2 offset a sedimentary succession comprising sands and shales (Fig. 9). Notable variations in fault throws are recorded when the fault segments in the sand-rich intervals are compared to fault segments in the shale-rich intervals. In the sand-rich intervals, fault throws are larger and range between 14 ms to 28 ms compared to the throw values between 2 ms to 10 ms of the shale rich-intervals (Fig. 9). A gradual trend in decrease of fault throw values is also noted as the faults propagate from sand-rich intervals into the shale-rich intervals (Fig. 9). Therefore, fault throws vary according to the mechanical character of specific intervals.

6. Mechanical character of interpreted seismic units

The bulk lithology of the interpreted seismic units can be ground-truthed, in the study area, by wells K15-01 and K15-04. This allowed us to compute the average interval velocity (Vp), depth, thickness, and competency ratio for the seismic units interpreted in this work.

Seismic Unit 5 is the main interval of interest - it forms a package of high-amplitude, high-frequency seismic reflections that is locally deformed by closely spaced normal faults (Figs. 6 and 7). For the purposes of this work, Unit 5 was sub-divided into three (3) sub-units, S5a, S5b and S5c, and subsequently classified into competent and incompetent intervals based on their lithology and competency ratios (Figs. 5 and 6; Table 2).

6.1 Well K15-01

6.1.1 Competent intervals

Competent seismic sub-units crossed by well K15-01 include S5a and S5c (Fig. 5). Sub-unit S5a is a package with moderate to high-amplitude, high-frequency seismic reflections that is unconformable over Unit S4 (Altena Group) (Fig. 5). Sub-unit 5b is a sand-rich interval interbedded with thin shales lenses. It as a Vp of 2650 m/s, a thickness of 371 m in well K15-01 and a relatively high competency ratio of 1.12 (Fig. 5; Table 2).

Internally, sub-unit S5c comprises a package with high-amplitude, high-frequency seismic reflections that is deformed by closely spaced normal faults (Fig. 5). This sub-unit is bounded at its top by the Base Tertiary horizon (H6), where an erosion maximum took place along the hinge of the main anticline (Figs. 5 and 6). Sub-unit S5c is predominantly sandy and characterised by its relatively high internal Vp of 2693 m/s. It is c. 404 m thick with a relatively high competency ratio of 1.23 (Figs. 5 and 6; Table 2).

Based on these data, we interpret sub-units S5a and S5c as competent intervals as they are predominantly sandy, present relatively high interval velocities between 2650 m/s and 2693 m/s, and a competency ratio between 1.12 and 1.23, i.e. higher than 1.0 (Fig. 5; Table 2).

6.1.2 Incompetent intervals

Incompetent intervals crossed by well K15-01 include Unit S4 and sub-unit S5b (Fig. 5). Unit S4 correlates with the Altena Group and is characterised by its high-amplitude, high-frequency seismic reflections (Fig. 5). This unit is shale-rich with a relatively low interval velocity of 2178 m/s. It also has a relatively low competency ratio of 0.87 for a total thickness of c. 528 m (Fig. 5; Table 2).

Sub-unit S5b is marked by its high-amplitude, high-frequency seismic reflections (Fig. 5). This package contains shales intercalated with thin layer of sands. The unit is characterised by its low Vp values (2370 m/s) and relatively low competency ratio of 0.88. Its thickness reaches 260 m (Fig. 5; Table 2).

Unit S4 and sub-unit S5b are interpreted as incompetent intervals due to being shaley with relatively low interval velocities between 2178 m/s and 2370 m/s, and by returning competency ratios <1.0 (Fig. 5; Table 2).

6.2 Well K15-04

6.2.1 Competent intervals

Competent intervals crossed by well K15-04 include sub-unit S5c, and interval with high-amplitude, high-frequency seismic reflections that is also sand-rich (Fig. 6). It has a relatively high Vp of 2638 m/s, a thickness of 342 m and a competency ratio of 1.25 (Fig. 6; Table 2).

6.2.2 Incompetent intervals

Incompetent units crossed by well K15-04 include Units S4, and sub-units S5a and S5b. They all comprise moderate- to high-amplitude, high-frequency internal reflections (Fig. 6). Low interval velocities (Vp) of 2067 m, 2120 m, and 2450 m are respectively recorded by Unit S4, sub-unit S5a and sub-unit S5b. These values result in relatively low competency ratios of 0.75 m, 0.87 and 0.90 (Fig. 6; Table 2). Unit S4 and sub-unit S5a comprise shale-rich intervals that are respectively 517 m and 212 m in thickness. The younger sub-unit S5b contains alternating sands and shales intervals for a thickness of 270 m (Fig. 6; Table 2). All these units are characterised by a relatively low competency ratio between 0.75 and 0.90.

7. Fault throw distributions through the interpreted mechanical units

Figures 9 and 10 show representative Faults F1, F2, F3, F4 and F5 that offset Upper Jurassic to Early Cretaceous strata. Important variations in fault throw are recorded across the identified competent and incompetent intervals (Figs. 9 and 10).

7.1 Well K15-01

Faults F1 and F2 are near well K15-01 and offset Late Jurassic-Early Cretaceous strata in Seismic Unit S4, and sub-units S5a, S5b and S5c (Fig. 5). Correlating the recorded Fault F1 throw values with distinct lithologies and competency ratios it becomes obvious that the competent sand-rich intervals (sub-units S5a and S5c), record relatively large fault throws between 31.8 m and 31.5 m (Fig. 9a). These values contrast with the smaller fault throw of 9.8 m that is recorded in the incompetent, shale-rich sub-unit S5b (Fig 9a; Table 2).

In a similar fashion, Fault F2 offsets Unit S4 and sub-units S5a, S5b and S5c. In the competent sand-rich intervals (sub-units S5a and S5c), are recorded large fault throws between 22.4 m and 21.3 m. Smaller fault throws between 5.20 m and 8.50 are recorded in the incompetent (shale-rich) sub-units S4 and S5b (Fig 9b; Table 2).

7.2 Well K15-04

Faults F3, F4 and F5 occur near well K15-04 (Fig. 6). These faults offset Jurassic-Cretaceous strata in Unit S4, and sub-units S5a, S5b and S5c. Once again, competent sand-rich intervals in sub-unit S5c record fault throws of 36.3 m, 41.1 m, and 38.3 m respectively for Faults F3, F4 and F5. In the incompetent sub-unit S5a, which is also shaley, smaller fault throws of 13.3 m, 15.9 m and 14.0 m were respectively recorded for F3, F4 and F5 (Figs. 10; Table 2).

In sub-unit S5b, which is composed of intercalated sand-shale intervals, fault throws of 18.2 m, 19.6 m and 17.3 m were recorded for Faults F3, F4 and F5. These values contrast with the larger fault throws of 36.3 m, 41.1 m, and 38.3 m of the more competent, and sandy, sub-unit S5c (Fig 10; Table 2). Consequently, a gradual decrease in fault throw values is recorded as the faults propagate from competent sand-rich sub-unit S5c into the incompetent shale-rich sub-unit 5b (Figs. 9 and 10).

8. Discussion

8.1 Fault geometries associated with the *horizontal shortening of outer-arc regions of folds*

In the BFB, Late Cretaceous to Miocene tectonic inversion (shortening) affecting Northwest Europe induced a continuum of deformation, leading to the generation, and subsequent reactivation, of pre-existing fault systems in reservoirs and adjacent overburden rocks (De Lugt et al., 2003; Ward et al., 2016; Maunde and Alves, 2022). This impacted their compartmentalisation styles, as tectonic movements reactivated pre-existing faults and allowed the secondary migration of fluids into shallower strata (De Lugt et al., 2003; Ward et al., 2016). Moreover, tectonic inversion triggered the development of broad folds and their associated outer-arc extensional faults, as well as subsequent reactivation of these latter faults in subsequent deformation (inversion) stages (Figs. 5, 6 and 11).

The onset of Late Cretaceous Sub-Hercynian inversion triggered the buckling of overburden strata, leading to the formation of a broad anticline and their associated outer-arc extensional faults. These structures accommodated the buckling strain and local stress distributions in the centre of the BFB (Figs. 5, 6 and 11b). The progressive buckling and folding of Meso-Cenozoic (supra-salt) strata during an intermediate stage – the Paleogene Laramide inversion phase - reactivated and lengthened the early formed faults in the hinge region of the broad anticline (Fig. 11c). The truncation of upper tip lines for these latter faults at horizon H6 signifies they were active near the hinge region of the broad anticline before the onset of the main erosional event (Figs. 5, 6 and 11c). Subsequently, the later Post-Miocene Pyrenean and Savian inversion episodes reactivated and lengthen some of these outer-arc faults into Tertiary strata (Fig. 11d).

The throw-depth profiles of Faults F1 to F5 show truncation at seismic horizon H6, at the same time they terminate downwards within Unit S4 (Figs. 9 and 10). These throw-depth profiles do not always have single positive gradients and are characterised by throw profiles that resemble a C-type pattern between the upper-tip point and immediate throw minima (Baudon and Cartwright, 2008; Maunde and Alves, 2020). The lack of near-zero throw values at seismic horizon H6 (base Tertiary boundary), confirms the erosion of the fault tips by Late Cretaceous to Paleogene erosion (Figs. 9, 10 and 11).

The fault-throw distribution of Faults F1 to F5 with depth is illustrated in Figs. 9 and 10 with reference to the throw-depth distributions. Fault segments or zones with local throw maxima (A segments) indicate the depth intervals or regions where pre-existing faults nucleated first within more competent intervals. Each segment (A) of these pre-existing faults propagates up-dip and/or down-dip to coalesce with other pre-existing fault segments that are in similar dip and/or strike directions to form a larger fault trace (Figs. 9 and 10). Linkage points of these pre-existing fault segments occur within the incompetent unit with local throw minima (B segments).

The character of these throw-depth profiles reflects vertically segmented fault arrays and fault growth by segment linkage, i.e. where two pre-existing separate faults with throw maxima (A) have propagated towards each other and linked together with a local throw minimum. Multiple local throw peaks on throw-depth profiles show that fault segmentation and linkage is a common process (Figs. 9 and 10). The similarity between the dips and strikes of these fault segments, nucleating at different depths, points out to one of the key characteristics of fault reactivation by segment linkage (Maunde and Alves, 2020; Baudon and Cartwright, 2008). Therefore, the results of the interpretation fault throw-depth support the concept that vertically segmented fault arrays initially nucleate first with larger fault throw (A segments) in competent units and are later linked by smaller fault throw (B segments) faults in less competent units (Peacock and Sanderson, 1992; Childs et al., 1996).

8.2 Mechanical controls on the geometry of outer-arc faults

Previous studies on tectonic fault evolution have revealed that, as strain accrues in a sedimentary succession, more competent strata fracture first, whereas incompetent strata fracture later (Ferrill and Morris, 2003, 2008; Welch et al., 2009) (Fig. 13). Thus, fractures are anticipated to initiate first in more competent sedimentary layers with throw maxima and are later radially propagate outwards to linked with adjacent pre-existing faults in less competent strata with throw minimum (Fig. 12). More recently, Libak et al. (2019) have shown that fault traces are more segmented in the less competent (claystones) layers, whereas more competent (sandy) layers have fault traces that record less segmentation and are more localised. Thus, faults tend to be less segmented (localized) with larger fault throw in more competent layers, and more segmented (deformation is less focused) in more ductile layers. Research has also shown that fault traces are steeper in the more competent layers, while being gentler in the less competent layers, a characteristic that leads to fault refraction (Ferrill et al. 2017; Peacock 2002). Also, Roche et al. (2012, 2013) showed that fault geometry is controlled by the thickness and competence of mechanical strata as well as the magnitudes of tectonic shortening, as observed in this study.

The throw-depth data in Figs. 9 and 10, illustrated the mode of reactivation and growth histories of the interpreted normal faults in the study area. Regions with larger fault throw (A segments) represent zones where faults nucleate early in more competent strata with throw maxima (Fig. 13a). Each segment/zone of these latter faults propagates outwards until they encounter adjacent fault segments and link- together (Fig. 13a,b). Linkage zones are situated where smaller fault throws (B segments) are documented in incompetent strata with throw minima (Fig. 13b,c). Therefore, zones with larger fault throw (Segments A) in the throw distribution profiles are interpreted as the locus of fault nucleation, which dominantly occurs in more competent intervals (Ferrill and Morris, 2008; Welch et al., 2009) (Figs. 9, 10, 12 and 13a).

Once a fault nucleates in more competent layers with throw maxima (Fig. 13a), the degree of fault growth is controlled by the mechanical behaviour and thickness of the rock (Roche et al., 2012, 2013). This behaviour is connected to the competence of the rock (Fig. 12) - incompetent rock (i.e. high ductile rock) will tend to hinder fault reactivation and growth, whereas competent (i.e. low ductile rock) will tend to fracture easily (Ferrill et al., 2017). In more competent layers such as chalk and sandstones, faults tend to rapidly propagate, whereas fault propagation and growth tend to slow in less competent layers such as mudstones (Ferrill and Morris, 2008; Ferrill et al., 2017) (Fig. 12). Faults that nucleate within a more competent rock interval may rapidly propagate outward until they encounter less competent rock interval and slow down (Fig. 13b). Therefore, vertical segmented fault throw arrays are likely to be noticeable, having established where faults are repressed from propagating into less competent intervals or layers (Fig. 13b, c).

In the interpreted throw-depth data in Figs. 9 and 10, we observed evidence for fault throw segmentation where the fault zones with smaller throw (B segments) in the less competent layers linked the pre-existing fault segments with larger fault throw (A segments) in the more competent layers (Figs. 9, 10 and 13). Less competent (ductile) layers can impede the propagation of faults from other layers, so that the point of deformation can be shifted laterally across the ductile layers. Such a shift in fault position across ductile layer can result in fault segmentation, whereby the fault segments can be hard or soft-linked (Gabrielsen et al., 2016; Maunde and Alves, 2021) (Figs. 9, 10 and 13).

Consequently, nucleation and subsequent propagation of fault slip from fault segments with larger throw (A segments) in the more competent layers, into the less competent layers, can define the anomalous and segmented fault throw arrays observed in the throw distribution data (Figs. 9, 10 and 13). The throw-depth (T-z) interpretation support the opinion that segmented fault throw arrays firstly nucleate in the more competent layers or intervals with zones of local throw maxima (A segments) and are later linked by faults in the less competent layers or intervals with zones of local throw minima (B segments) (Ellis and Dunlap, 1988; Maunde and Alves, 2022) (Fig. 13).

On the interpreted seismic sections, there is no noticeable structural expression for vertically segmented fault arrays equivalent to that shown in the schematic section of Fig. 13 or changes in fault dip geometries as faults propagate from competent into incompetent intervals (Figs. 5, 6, 9 and 10). This is because the faults are not resolved by the processed seismic dataset, and the initial segment dip-linkage faults have been distorted during post-linkage slip on the fault and also, fault segments merged during their propagation and growth, a character resulting in the adjusting of the active fault trace. Therefore, although seismic dataset may not well resolve the local faults in wholly satisfactory way, the mechanical control of these faults may leave its signature as distinct fault-throw regions (A and B segments), which can be detected through high resolution throw-depth (T-z) mapping, as shown in Figs. 9 and 10.

9. Conclusions

The conclusions derived from the detailed mapping of normal faults and their throws, combined with the identification of mechanical units in the BFB, can be summarised as follows:

a) Closely spaced and more localised fault arrays with narrow deformation zones are observed in relatively competent, sand-rich strata. In contrast, widely spaced and less localised fault arrays with wider deformation zones occur in the more incompetent shale-rich intervals.
b) The high-resolution throw-depth mapping developed in this work shows that vertically segmented/anomalous fault throw arrays were initially nucleated in the more competent intervals, i.e. those presenting the larger fault throws. They were later linked to faults in the less competent intervals, which show relatively small fault throws. Thus, fault throw geometry can provide information about variations in the mechanical behaviour of rock units.
c) Anomalous fault-throw distributions indicate fault growth through segment linkage. Hence, multiple pre-existing faults with larger fault throws propagated towards each other and were linked in the areas where throw minima are recorded.
d) A consequence of fault reactivation and growth through linkage was the formation of large-scale fault traces at advanced stages. Fault linkages and intersections are important for the accumulation and trapping of fluids. Although they may lead to an overall increased in effective permeability and can thus act as vertical conduits for fluid migration into traps, they also have negative effect on seal integrity.

On the interpreted seismic sections, seismic dataset may not well resolve the local faults in wholly satisfactory way, but the mechanical control of these faults may still leave an inherited signature in fault throws (regions A and B; Figs. 9 and 10). These correspond to the regions where faults linked and can still be detected through high resolution mapping of throw-depth (T-z) data along outer-arc faults. Hence, to recognise the mechanical controls on fault geometry is a vital component of characterising both faulted hydrocarbon reservoirs and mineral provinces.

Declaration of competing interest

The authors declare that they have no known competing financial interests or personal relationships that could have appeared to influence the work reported in this paper.

Acknowledgements

Petroleum Technology Development Fund (PTDF), Nigeria was acknowledged and thanked for funding the research study. We acknowledge the permission approved by Haloil and CGG-Veritas for the use of the seismic data included in this article and Schlumberger for the provision of seismic interpretation software (Petrel). This paper is dedicated to Richard J. Lisle, who introduced the second author TM Alves to impressive examples of outer-arc faults, back in the 2000s, in Northern Spain. Wish we had been given the time to find more outer-arc faults in many more field trips.

Author contributions

AM: Conceptualization, Investigation, Methodology, Writing – original draft. TA: Formal analysis, Project administration, Resources, Software, Supervision, Validation, Writing – review and editing.

References

Alves, T. M., 2012. Scale-relationships and geometry of normal faults reactivated during gravitational gliding of Albian rafts (Espírito Santo Basin, SE Brazil). Earth and Planetary Science Letters, 331, 80-96.

Alves, T.M., Cartwright, J.A., 2010. The effect of mass-transport deposits on the younger slope morphology, offshore Brazil. Mar. Pet. Geol. 27, 2027–2036.

Alves, T.M., Elliott, C., 2014. Fluid flow during early compartmentalisation of rafts: a North Sea analogue for divergent continental margins. Tectonophysics 634, 91–96.

Alves, T. M., Taylor, J., Corcorant, p., Tao, Z., 2025. Data sampling strategies for accurate fault analyses: A scale-independent test based on a machine learning approach. Journal of Structural Geology, 191, 105342

Asmus, H.E., Gomes, J.B., Pereira, A.C.B., 1971. Integraçao geologica regional da bacia do Espírito Santo. Relatorio Interno, PETROBRAS.

Baudon, C., Cartwright, J., 2008. The kinematics of reactivation of normal faults using high resolution throw mapping. Journal of Structural Geology, 30, 1072-1084.

Bentham, M., Green, A., Gammer, D., 2013. The occurrence of faults in the Bunter Sandstone Formation of the UK sector of the Southern North Sea and the potential impact on storage capacity. Energy Procedia 37, 5101–5109.

Barnett, J.A., Mortimer, J., Rippon, J.H., Walsh, J.J., Watterson, J., 1987. Displacement geometry in the volume containing a single normal fault. AAPG Bull. 71, 925–937.

Barker, P.F., Buffler, R.T., Gambôa, L.A., 1983. A seismic reflection study of the Rio Grande Rise. In: Barker, P.F., Carlson, R.L., Hohnson, D.A. (Eds.), Initial Reports of the Deep Sea Drilling Program, 72. U.S. Government Printing Office, Washington, pp. 499–517.

Brandes, Ch., Tannerr, D.C. 2014. Fault-related folding: A review of kinematic models and their application. Earth-Sci. Rev. 138, 352-370. https://doi.org/10.1016/j.earscirev.2014.06.008

Cartwright, J. A., Trudgill, B. D., Mansfield, C. S. 1995. Fault growth by segment linkage: An explanation for scatter in maximum displacement and trace length data from the Canyonlands Grabens of SE Utah. Journal of Structural Geology, 17, 1319-1326.

Cartwright, J., Huuse, M., Aplin, A., 2007. Seal bypass systems. American Association of Petroleum Geologists Bulletin 91 (8), 1141–1166

Caine, J.S., Evans, J.P., Forster, C.B., 1996. Fault zone architecture and permeability structure. Geology, 24, 1025–1028.

Childs, C., Watterson, J., Walsh, J. 1995. Fault overlap zones within developing normal fault systems. Journal of the Geological Society, 152, 535-549.

Coward, M., 1995. Structural and Tectonic Setting of the Permo-Triassic Basins of Northwest Europe, vol. 91. Geological Society, London, Special Publications, pp. 7–39.

Chang, H.K., Kowsmann, R.O., Figueiredo, A.M.F., Bender, A., 1992. Tectonics and stratigraphy of the East Brazil Rift system: an overview. Tectonophysics 213, 97–138.

Cowie, P. A. and Scholz, C. H. 1992. Growth of faults by accumulation of seismic slip. J. geophys. Res. 97(B7), 11,085-11,095.

Dawers, N.H., Anders, M.H., 1995. Displacement-length scaling and fault linkage. Journal of Structural Geology. 17, 607–614.

De Lugt, I.R., Van Wees, J.D., Wong, T.E., 2003. The tectonic evolution of the southern Dutch North Sea during the Palaeogene: basin inversion in distinct pulses. Tectonophysics 373, 141–159.

Demercian, S., Szatmari, P., Cobbold, P., 1993. Style and pattern of salt diapirs due to thin-skinned gravitational gliding, Campos and Santos basins, offshore Brazil. Tectonophysics 228, 393–433.

Duin, E., Doornenbal, J., Rijkers, R., Verbeek, J., Wong, T.E., 2006. Subsurface structure of The Netherlands-results of recent onshore and offshore mapping. Neth. J. Geosci. 85, 245.

Ellis, M. A., Dunlap, W. J. 1988. Displacement variation along thrust faults: Implications for the development of large faults. Journal of Structural Geology, 10, 183-192.

Ferrill, D.A., McGinnis, R.N., Morris, A.P., McGinnis, R.N., Smart, K.J., Wigginton, S. S., Hill, N.J., 2017. Mechanical stratigraphy and normal faulting. Review article. J. Struct. Geol. 94, 275-302.

Ferrill, D.A., Morris, A.P., 2003. Dilational normal faults. Journal of Structural Geology. 25, 183-196.

Fiduk, J.C., Brush, E.R., Anderson, L.E., Gibbs, P.B., Rowan, M.G., 2004. Salt deformation, magmatism, and hydrocarbon prospectivity in the Espirito Santo Basin, offshore Brazil. In: Salt-sediment Interactions and Hydrocarbon Prospectivity: Concepts, Applications, and Case Studies for the 21st Century: Proceedings of Gulf Coast Section SEPM Foundation Bob F. Perkins Research Conference, 2004. SEPM, pp. 370–392.

Ferrill, D.A., Morris, A.P., 2008. Fault zone deformation controlled by carbonate mechanical stratigraphy, Balcones fault system, Texas. AAPG Bull. 92, 359-380.

França, R.L., Del Rey, A.C., Tagliari, C.V., Brandao, J.R., Fontanelli, P.D.R., 2007. Bacia do Espírito Santo. Bol. Geociencias Petrobras 15, 501–509.

Gabrielsen, R.H., Sokoutis, D., Willingshofer, E., Faleide, J.I. 2016. Fault linkage across weak layers during extension: an experimental approach with reference to the Hoop Fault Complex of the SW Barents Sea. Petroleum Geoscience, 22, 123–135.

Gamboa, D., Alves, T., Cartwright, J., Terrinha, P., 2010. MTD distribution on a 'passive'continental margin: the Espírito Santo Basin (SE Brazil) during the Palaeogene. Mar. Pet. Geol. 27, 1311–1324.

Gerling, P., Geluk, M., Kockel, F., Lokhorst, A., Lott, G., Nicholson, R., 1999. ’NW European Gas Atlas’–new implications for the Carboniferous gas plays in the western part of the Southern Permian Basin. In: Geological Society, London, Petroleum Geology Conference Series, 1999. Geological Society of London, pp. 799–808.

Gibbs, P.B., Brush, E.R., Fiduk, J.C., 2003. The Evolution of the Syn Rift and Transition Phases of the Central/southern Brazilian and W. African Conjugate Margins: The Implications for Source Rock Distribution in Time and Space, and Their Recognition on Seismic Data. 8th International Congress of the Brazilian Geophysical Society, Brazil. September 14-18, 2003.

Kim, Y.-S., Sanderson, D.J., 2005. The relationship between displacement and length of faults: a review. Earth-Sci. Rev. 68, 317–334.

Kim, Y.-S., Andrews, J.R., Sanderson, D.J., 2000. Damage zones around strike-slip fault systems and strike–slip fault evolution, Crackington Haven, southwest England. Geoscience Journal 4, 53-72.

Li, T., Chen, J., Thomson Jobe, J.A., Burbank, D.W., Cheng, X., Xu, J., Li, Z., Zheng, W., Zhang, P., 2018. Active bending-moment faulting: Geomorphic expression, controlling conditions, accommodation of fold deformation. Tectonics 37, 2278-2306. https://doi.org/10.1029/2018TC004982

Libak, A., Torabi, A., Alae, B., 2019. Normal fault geometric attribute variations with lithology: examples from the Norwegian Barents Sea. Geological Society London Special Publications, 495, DOI: 10.1144/SP495-2018-164.

Lohr, T., Krawczyk, C.M., Oncken, O., Tanner, D.C., 2008. Evolution of a fault surface from 3D attribute analysis and displacement measurements. J. Struct. Geol. 30, 690–700.

Mansfield, C.S., Cartwright, J.A., 1996. High resolution fault displacement mapping from three-dimensional seismic data: evidence for dip linkage during fault growth. Journal of Structural Geology. 18, 249–263.

Mansfield, C., Cartwright, J., 2001. Fault growth by linkage: observations and implications from analogue models. J. Struct. Geol. 23, 745–763.

Maunde. A., Alves. T.M., Moore, G. F., 2021. Shallow fault systems of thrust anticlines responding to changes in accretionary prism lithology (Nankai, SE Japan). Tectonophysics 812 (2021) 228888.

Maunde, A., Alves, T.M., 2020. Impact of tectonic rafts' gravitational instability on fault reactivation and geometry. J. Struct. Geol. 130 (2020) 103916.

Maunde, A., Alves, T.M., 2022. Effect of tectonic inversion on supra-salt fault geometry and reactivation histories in the Southern North Sea. Marine and Petroleum Geology. 135 (2022) 105401.

McClay, K. R. 1990. Extensional fault systems in sedimentary basins: a review of analogue model studies. Marine and Petroleum Geology, 7, 206–233.

Mitra, S., 2022. Fold-accommodation faults. AAPG Bull. 86, 671-693. https://doi.org/10.1306/61EEDB7A-173E-11D7-8645000102C1865D

Mohriak, W.U., 2003. Bacias sedimentares da margem continental Brasileira. In: Bizzi, L. A., Schobbenhaus, C., Vidotti, R.M., Goncalves, J.H. (Eds.), Geologia, Tectonica e Recursos Minerais do Brasil. CPRM, Brasilia, pp. 87–165.

Mohriak, W., Nemcok, M., Enciso, G., 2008. South Atlantic divergent margin evolution: rift-border uplift and salt tectonics in the basins of SE Brazil. Geol. Soc. Lond. Spec. Publ. 294, 365–398.

Mohriak, W.U., Palagi, P.R., Mello, M.R., 1998. Tectonic evolution of south Atlantic salt basins. AAPG Bull. 82 (10), 1945.

Nalpas, T., Le Douaran, S., Brun, J.P., Unternehr, P., Richert, J.P., 1995. Inversion of the Broad Fourteens Basin (offshore Netherlands), a small-scale model investigation. Sediment. Geol. 95, 237–250.

Nicol, A., Walsh, J., Berryman, K., Nodder, S., 2005. Growth of a normal fault by the accumulation of slip over millions of years. Journal of Structural Geology 27 (2), 327 342.

Ojeda, H., 1982. Structural framework, stratigraphy, and evolution of Brazilian marginal basins. AAPG (Am. Assoc. Pet. Geol.) Bull. 66, 732–749.

Oudmayer, B.C., De Jager, J., 1993. fault reactivation and oblique slip in the Southern North Sea. In: Parker, J.R. (Ed.), Petroleum Geology of Northwest Europe: Proceedings of the 4th Conference, 1993 London. The Geological Society, pp. 1281–1290.

Peacock, D.C.P., 2002. Propagation, interaction and linkage in normal fault systems. Earth Sci. Rev. 58, 121–142.

Peacock, D.C.P., Sanderson, D.J., 1991. Displacements, segment linkage and relay ramps in Normal fault zones. Journal of Structural Geology. 13, 721–733.

Penge, J., Munns, J.W., Taylor, B., Windle, T.M.F., 1999. Rift-raft tectonics: examples of gravitational tectonics from the Zechstein basins on northwest Europe. In: Fleet, A.J., Boldy, S.A.R. (Eds.), Petroleum Geology of Northwest Europe, Proceedings of the 5th Conference, pp. 201–213.

Pollard, D. D., Segall P., 1987. To faults, joints, veins and solutions. Fractures Mechanics of Rocks. Pp 277. Academic Press.

Ramsay, J.G., 1967. Folding and Fracturing of Rocks. McGraw-Hill Book Company, New York. 07-051170-5.

Roche, V., Homberg, C., Rocher, M., 2012. Architecture and growth of normal fault zones in multilayer systems: a 3D field analysis in the South-Eastern Basin, France. J. Struct. Geol. 37, 19-35.

Roche, V., Homberg, C., Rocher, M., 2013. Fault nucleation, restriction, and aspect ratio in layered sections: quantification of the strength and stiffness roles using numerical modeling. J. Geophys. Res. Solid Earth 118, 1-15.

Schlische, R.W., 1995. Geometry and origin of fault-related folds in extensional settings. AAPG Bull. 79, 1661-1678. https://doi.org/10.1306/7834DE4A-1721-11D7-8645000102C1865D

Tao, Z., Alves, T.M., 2019. Impacts of data sampling on the interpretation of normal fault propagation and segment linkage. Tectonophysics 762, 79–96.

Van Hulten, F.F.N., 2010. Geological Factors Effecting Compartmentalization of Rotliegend Gas Fields in the Netherlands, vol. 347. Geological Society, London, Special Publications, pp. 301–315.

Van Verweij, J.M., Simmelink, H.J., 2002. Geodynamic and hydrodynamic evolution of the Broad Fourteens Basin (The Netherlands) in relation to its petroleum systems. Mar. Petrol. Geol. 19, 339–359.

Van Wees, J.-D., Stephenson, R., Ziegler, P., Bayer, U., McCann, T., Dadlez, R., Gaupp, R., Narkiewicz, M., Bitzer, F., Scheck, M., 2000. On the origin of the southern Permian Basin, central Europe. Mar. Petrol. Geol. 17, 43–59.

Van Wijhe, D.V., 1987. Structural evolution of inverted basins in the Dutch offshore. Tectonophysics 137, 171–219.

Walsh, J., Nicol, A., Childs, C. 2002. An alternative model for the growth of faults. Journal of Structural Geology, 24, 1669-1675.

Walsh, J.J., Watterson, J., 1988. Dips of normal faults in British Coal Measures and other sedimentary sequences. J. Geol. Soc. Lond. 145, 859-873.

Ward, N.I., Alves, T.M., Blenkinsop, T.G., 2016. Reservoir leakage along concentric faults in the Southern North Sea: Implications for the deployment of CCS and EOR techniques. Tectonophysics 690, 97-116

Welch, M.J., Davies, R.K., Knipe, R.J., Tueckmantel, C., 2009. A dynamic model for fault nucleation and propagation in a mechanically layered section. Tectonophysics 474, 473-492.

Wilkins, S.J., Gross, M.R., 2002. Normal fault growth in layered rocks at Split Mountain, Utah: influence of mechanical stratigraphy on dip linkage, fault restriction and fault scaling. Journal of Structural Geology 24 (9), 1413–1429.

Wong, T.E., Parker, N., Horst, P., 2001. Tertiary sedimentary development of the Broad Fourteens area, The Netherlands. Geol. Mijnbouw 80, 85–94.

Yeats, R. S., 1986. Active faults related to folding. *Active tectonics*, 63-79.

Ziegler, P.A., 1990. Geological Atlas of Western and Central Europe, Shell Internationale Petroleum. Maatschappij B.V., The Hague.

Figure captions

Fig. 1. Regional map of the Southern North Sea highlighting the Broad Fourteens Basin (BFB) and the location of the study area, Dutch offshore sector.

Fig. 2. Seismic-stratigraphic correlation amongst interpreted seismic units, well logs, main lithologies and the stratigraphic groups recognised in the Broad Fourteens Basin (BFB), Southern North Sea. Stratigraphic groups and main lithologies are based on Penge et al. (1999) and van Verweij and Simmelink. (2002). H1 to H6 and S1 to S7 are interpreted seismic horizons and units, respectively. GR refers to the vertical gamma-ray log responses through the stratigraphic-seismic units. K15-01 and K15-07 refer to the name/location of the wells analysed in this work.

Fig. 3. a) Uninterpreted and b) interpreted seismic profile highlighting the geometry of the broad (inversion) anticline of the Broad Fourteens Basin (BFB) and associated faults. Unit S5 is highly deformed by closely spaced normal faults at the hinge region of this broad anticline. These faults are mostly truncated upwards at the base of seismic horizon H6. Deeply rooted listric faults Units S3 and S4. Unit S6 was eroded at the hinge zone of the broad anticline.

Fig. 4. a) Uninterpreted and b) interpreted seismic profile showing Units S1 to S7 and associated structural features. Deeply rooted listric normal fault propagate vertically upwards into Unit S7 (Cenozoic strata), without reaching the seafloor. These faults are associated with the gravitational gliding of strata that sole-out in the Zechstein salt (Unit S2), which acts as a décollement layer (rift-raft tectonics cf. Penge et al., 1999). The high (green) GR readings are linked to a high shales content, whereas the low (purple) GR readings indicate that sands dominate in this intervals.

Fig. 5. Zoomed-in seismic profile highlighting the geometry of faults and the internal mechanical character of Seismic Unit S4, and sub-units S5a, S5b and S5c near well K15-01. Parameters of interest include lithology, interval velocity (Vp), seismic unit thickness and relative competence. From well K15-01 data, sub-units S5a and S5c comprise sandy intervals while sub-unit S5b comprises sandy intervals with thin interbedded layer of shale. Sub-units S5a and S5c show relatively high Vp values of 2650 m/s and 2693 m/s with a high competency ratio of 1.12 and 1.23, respectively. The softer Unit S4 and S5b show relatively low Vp values of 2078 m/s and 2370 m/s and low competency ratios between 0.78 and 0.88, respectively. The high (green) GR readings are linked to a high shales content, whereas the low (purple) GR readings indicate that sands dominate in this intervals. The red DT responses represent the sonic-log readings.

Fig. 6. Zoomed-in seismic profile showing the geometry of faults and mechanical character of Seismic Unit S4 and sub-units S5a, S5b and S5c near well K15-04. Parameters of interest include lithology, interval velocity (Vp), seismic unit thickness and relative competence. Seismic Unit S4 and sub-units S5a and S5b comprise shaley intervals with thin sand layers. They respectively record

Vp values of 2067 m/s, 2120 m/s, 2450 m/s and 2738 m/s, and competencies ratios of 0.75, 0.85 and 0.90. In contrast, sub-unit S5c shows a relatively high Vp of 2078 m/s and a relatively high competency ratio of 1.25. Sub-unit S5c is sand-rich. The high (green) GR readings are linked to a high shales content, whereas the low (purple) GR readings indicate that sands dominate in this intervals.

Fig. 7. TWTT structural maps and schematic interpretations of outer-arc faults offsetting seismic sub-unit S5b. a) TWTT structural map, b) zoomed-in TWTT structural map. The figure highlights the geometry expression faults propagating through more competent sand-rich intervals in sub-unit S5c. The imaged fault arrays are closely spaced, more localised, with narrow deformation zones. They are also linked, forming a curvilinear polygonal plan-form geometry. The faults have trace lengths of 1300–12000 m, a spacing of 320-1000 m, and throw maxima between 21 m and 41 m.

Fig. 8. TWTT structural maps and schematic interpretations of outer-arc faults offsetting sub-unit S5a, which is shaley and relatively incompetent. a) TWTT structural map, b) zoomed-in TWTT structural map. Here, faults are widely spaced and less localised, showing wider deformation zone. The faults have trace lengths of 1500–7,000 m, a spacing of 220-2000 m, and throw maxima between 13 m and 15 m.

Fig. 9. Representative vertical fault throw-depth (T-z) profiles for Faults F1 and F2 near well K15-01. a) Fault F1 and b) fault F2. These profiles show anomalous throw distributions along the interpreted faults. Correlations amongst fault throw distributions with lithologies and competency ratios derived from well K15-01 show that fault throws are greater (between 21.3 m and 38.8 m) in the sand-rich intervals of sub-units S5a and S5c. Shale-rich intervals present lower fault throws (between 5.2 m and 9.8 m) in Unit S4 and sub-unit S5b. Moreover, the more competent sand-rich intervals in sub-units S5a and S5c have a relatively competency ratio between 1.12 and 1.23 (i.e. > 1.0), compared to a relatively low competency ratio of between 0.78 and 0.88 (i.e. less than one) in the incompetent, shaley Units S4 and sub-unit S5b. In the Figure, zones represented by the letter A

are segments of faults with throw maxima between 21 m to 38 m. The letter B represent regions with throw minima between 6 m and 13 m.

Fig. 10. Representative vertical fault throw-depth (T-z) profiles for Faults F3, F4 and F5 near well K15-04. a) Fault F1, and b) fault F2. Unit S4, and sub-units S5a and S5b comprise shaley intervals with thin sand layers. They respectively have Vp velocities of 2067 m/s, 2120 m/s, 2450 m/s and 2738 m/s, resulting in competency ratios of 0.75, 0.85 and 0.90. In contrast, sub-unit S5c shows a relatively high Vp of 2078 m/s and a high competency ratio of 1.25, as it is a sand-rich interval. Correlating these differing mechanical characters (i.e. lithology and competency ratio)s with fault-throw distributions shows that faults F3, F4 and F5 have higher throws (between 36.3 m and 38.8 m), in the more competent sand-rich intervals. Lower fault throws between 5.2 m and 15.6 m are recorded in shaley rich-intervals. In the Figure, A segments are the regions representing throw maxima between 21 - 38 m, whereas B segments are regions with throw minima between 6 -13 m.

Fig. 11. Sketch summarising the geological evolution and geometric relationship between the broad anticline of the BFB and its associated outer-arc normal faults. a) Syn-rift phase (tectonic extension), b) early phase of tectonic inversion, c) later phase of tectonic inversion and shortening, and d) post-inversion phase.

Fig. 12. Diagram showing the relationships amongst mechanical character, fault throw, interval velocity and rock unit competency of particular stratigraphic intervals. Competent units are characterised by a relatively high interval velocity (Vp), larger fault-throw values and a relatively high competency ratio greater than one (> 1). In contrast, incompetent units are characterised by a relatively low interval velocity (Vp), smaller fault-throw values and a relatively low competency ratio (C<1). Rock competency is the ratio of a unit's interval velocity (Vp) to the adjacent unit's interval velocity. Interval velocity is a function of the strength and stiffness of a material (see sub-section 3.2.2 in this paper).

Fig. 13. Diagrams showing the evolution and growth histories of outer-arc normal faults in the study area. a) Faults nucleate early in more competent intervals with local zones of throw maxima (A), these early faults accumulate higher displacement and propagates radially outwards until they encounter other fault segments that are in similar strike and dip directions to link together. b) Linkage points are situated where throw minima (B) are recorded in less competent intervals. c) The linked segments rapidly accumulate displacement and thus reduce any differences in the throw distribution profiles. These modes of fault growth concur with fault growth via segment-linkage.

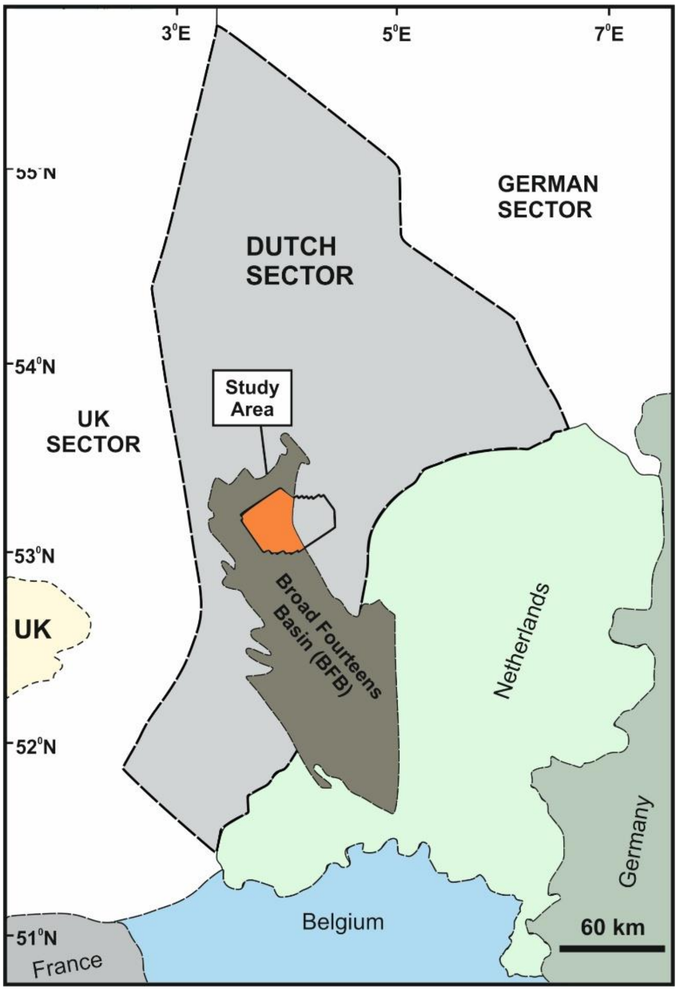
3°E
5°E
7°E
55°N
54°N
53°N
52°N
51°N
GERMAN SECTOR
DUTCH SECTOR
UK SECTOR
Study Area
UK
Broad Fourteens Basin (BFB)
Netherlands
Germany
Belgium
France
60 km

Fig. 1

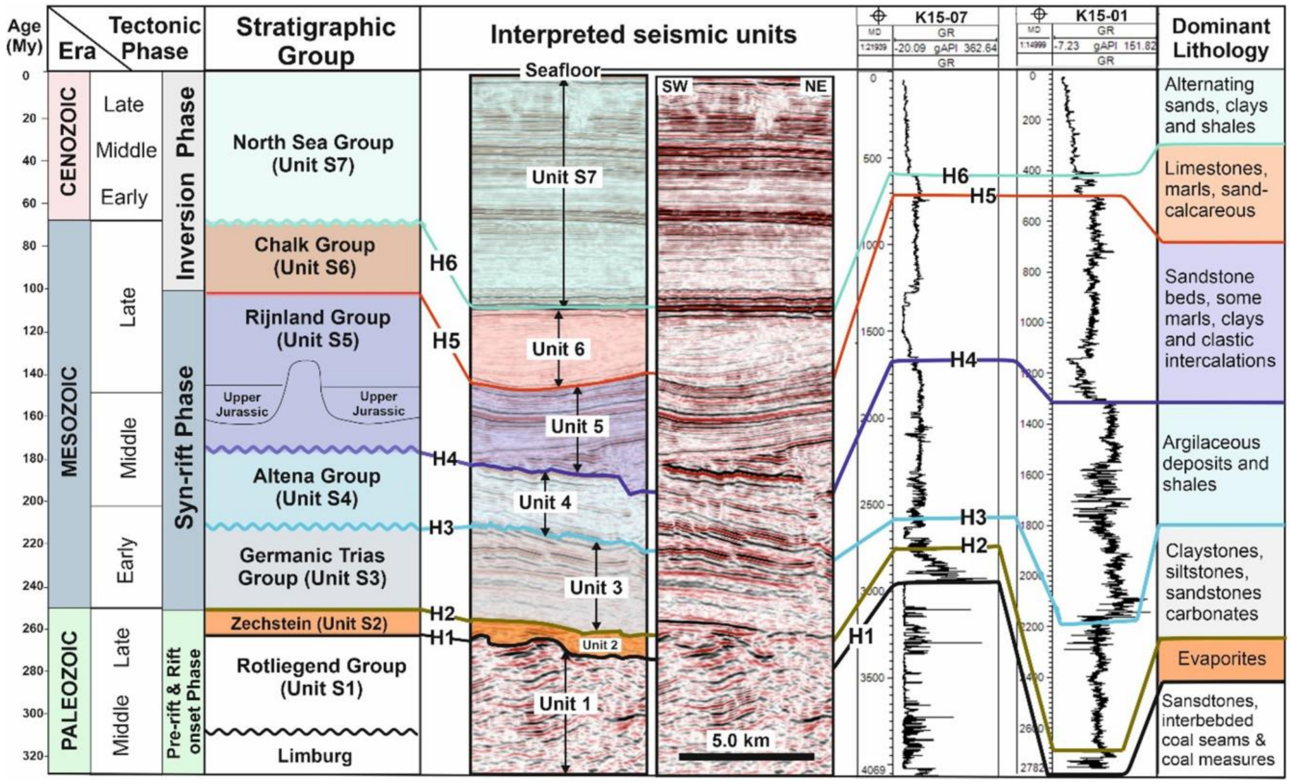

Age (My)
Era
Tectonic Phase
Stratigraphic Group
Interpreted seismic units
K15-07
K15-01
Dominant Lithology
CENOZOIC
MESOZOIC
PALEOZOIC
Late
Middle
Early
Inversion Phase
Syn-rift Phase
Pre-rift & Rift onset Phase
North Sea Group (Unit S7)
Chalk Group (Unit S6)
Rijnland Group (Unit S5)
Upper Jurassic
Upper Jurassic
Altena Group (Unit S4)
Germanic Trias Group (Unit S3)
Zechstein (Unit S2)
Rotliegend Group (Unit S1)
Limburg
Seafloor
Unit S7
Unit 6
Unit 5
Unit 4
Unit 3
Unit 2
Unit 1
SW
NE
5.0 km
H6
H5
H4
H3
H2
H1
Alternating sands, clays and shales
Limestones, marls, sand-calcareous
Sandstone beds, some marls, clays and clastic intercalations
Argilaceous deposits and shales
Claystones, siltstones, sandstones carbonates
Evaporites
Sansdtones, interbebded coal seams & coal measures

Fig. 2

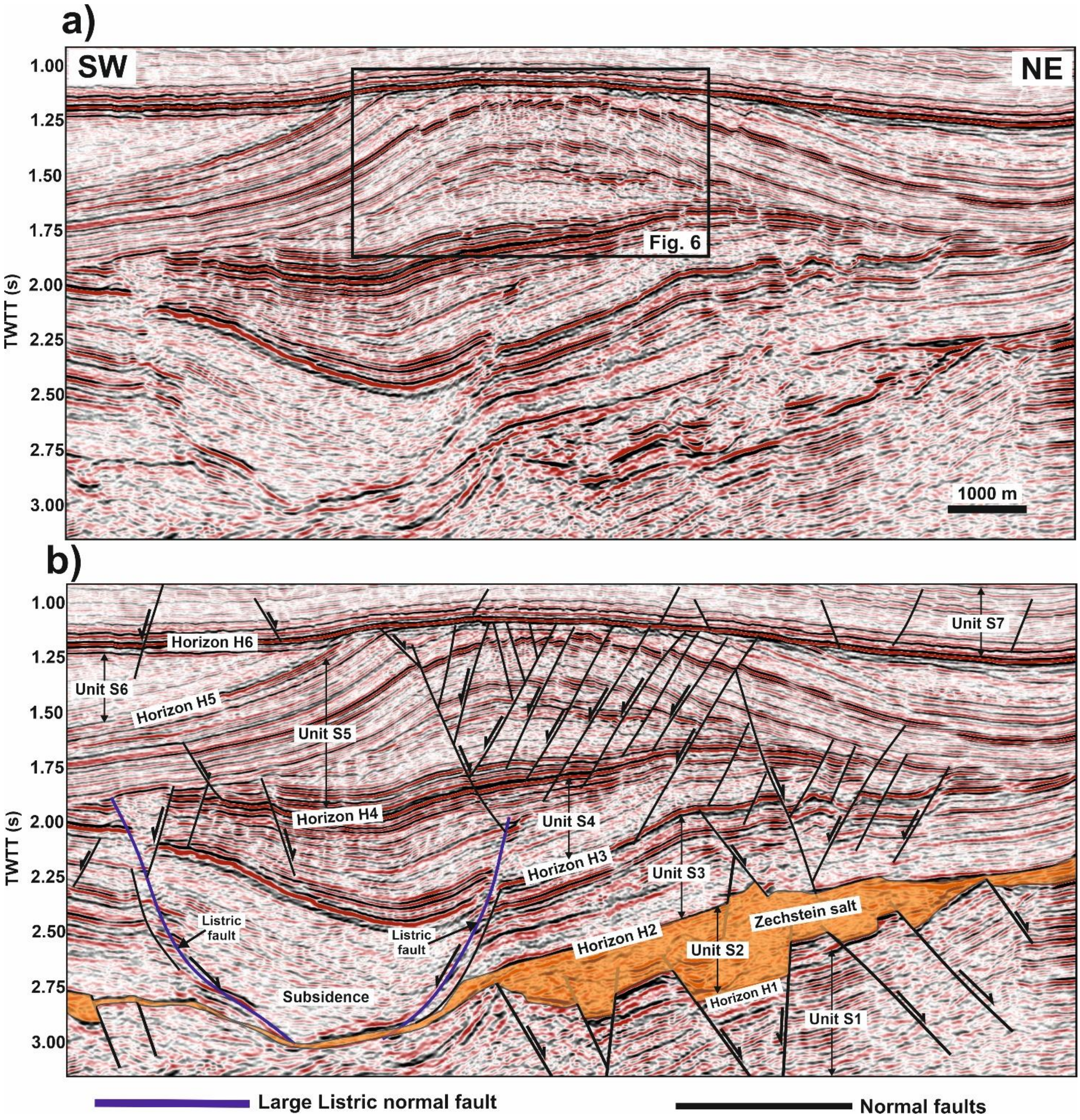
a)
SW
NE
1.00
1.25
1.50
1.75
2.00
2.25
2.50
2.75
3.00
TWTT (s)
Fig. 6
1000 m
b)
Horizon H6
Unit S6
Horizon H5
Unit S5
Unit S7
Horizon H4
Unit S4
Horizon H3
Unit S3
Listric fault
Listric fault
Subsidence
Horizon H2
Zechstein salt
Unit S2
Horizon H1
Unit S1
Large Listric normal fault
Normal faults

Fig. 3

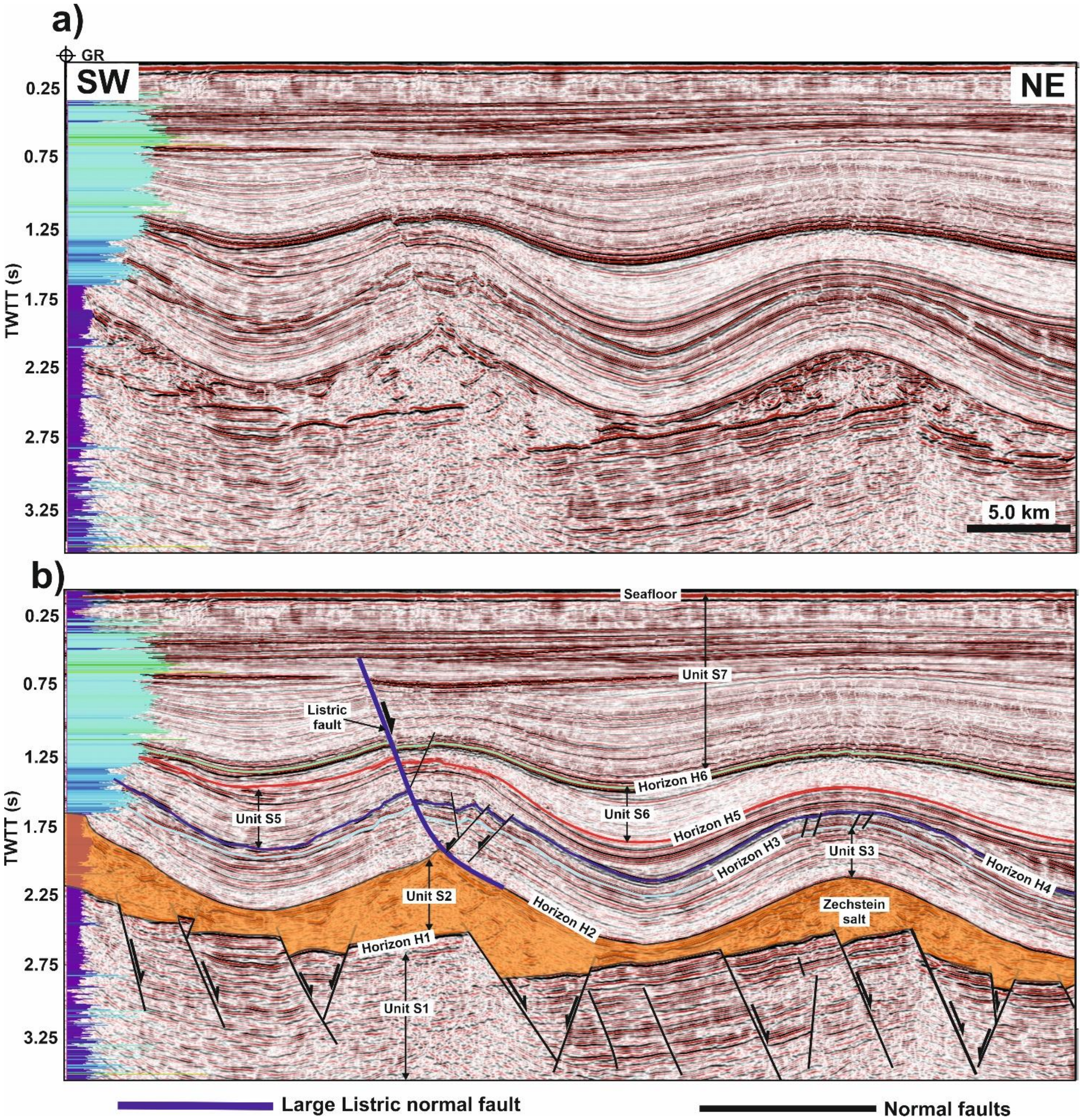
a)
GR
SW
NE
0.25
0.75
1.25
1.75
2.25
2.75
3.25
TWTT (s)
5.0 km
b)
Seafloor
Unit S7
Listric fault
Horizon H6
Unit S5
Unit S6
Horizon H5
Horizon H3
Unit S3
Horizon H4
Unit S2
Horizon H2
Zechstein salt
Horizon H1
Unit S1
Large Listric normal fault
Normal faults

Fig. 4

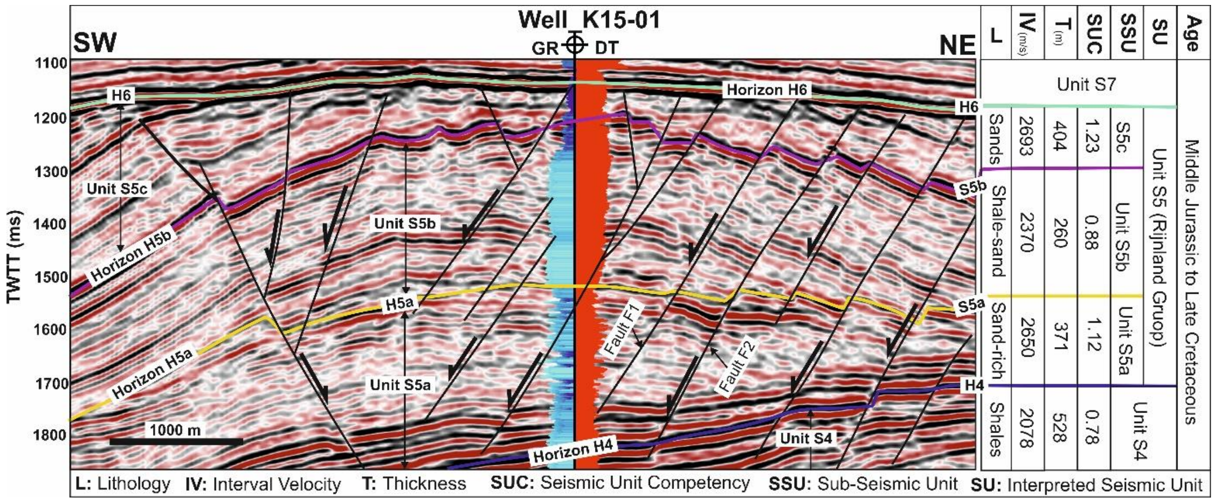

Well_K15-01
SW
NE
GR
DT
TWTT (ms)
1100
1200
1300
1400
1500
1600
1700
1800
H6
Horizon H6
Unit S5c
Horizon H5b
Unit S5b
H5a
Horizon H5a
Unit S5a
Fault F1
Fault F2
Horizon H4
Unit S4
1000 m
S5b
S5a
H4
L
IV (m/s)
T (m)
SUC
SSU
SU
Age
Unit S7
Sands
2693
404
1.23
S5c
Shale-sand
2370
260
0.88
Unit S5b
Sand-rich
2650
371
1.12
Unit S5a
Unit S5 (Rijnland Gruop)
Shales
2078
528
0.78
Unit S4
Middle Jurassic to Late Cretaceous
L: Lithology IV: Interval Velocity T: Thickness SUC: Seismic Unit Competency SSU: Sub-Seismic Unit SU: Interpreted Seismic Unit

Fig. 5

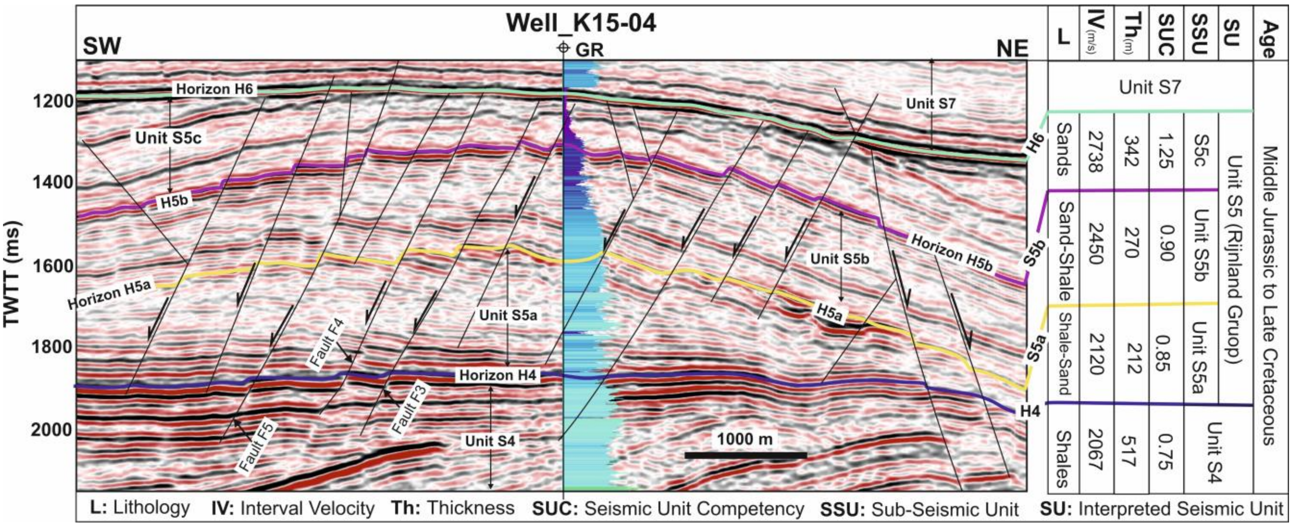
Well_K15-04
SW
GR
NE
L
IV (m/s)
Th (m)
SUC
SSU
SU
Age
TWTT (ms)
1200
1400
1600
1800
2000
Horizon H6
Unit S5c
H5b
Horizon H5a
Unit S5a
Fault F4
Fault F3
Fault F5
Horizon H4
Unit S4
Unit S7
Unit S5b
Horizon H5b
H5a
1000 m
H6
S5b
S5a
H4
Unit S7
Sands
2738
342
1.25
S5c
Sand-Shale
2450
270
0.90
Unit S5b
Shale-Sand
2120
212
0.85
Unit S5a
Unit S5 (Rijnland Gruop)
Shales
2067
517
0.75
Unit S4
Middle Jurassic to Late Cretaceous
L: Lithology IV: Interval Velocity Th: Thickness SUC: Seismic Unit Competency SSU: Sub-Seismic Unit SU: Interpreted Seismic Unit

Fig. 6

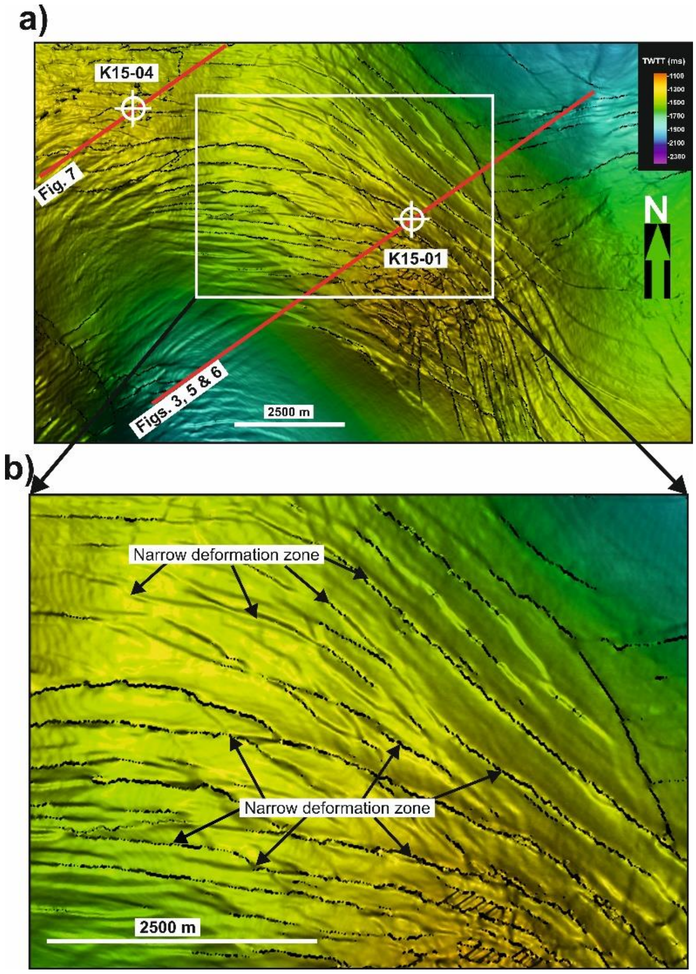
a)
K15-04
K15-01
Fig. 7
Figs. 3, 5 & 6
2500 m
TWTT (ms)
N
b)
Narrow deformation zone
Narrow deformation zone
2500 m

Fig. 7

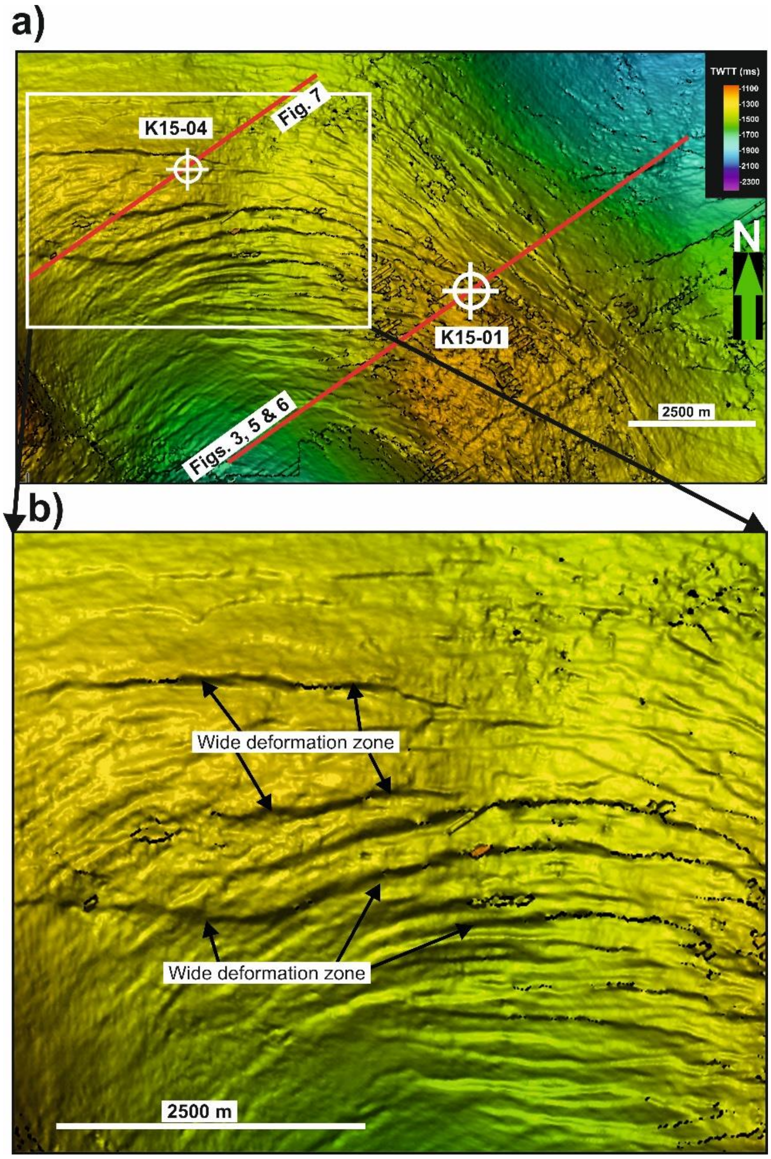
a)
TWTT (ms)
1100
1300
1500
1700
1900
2100
2300
N
K15-04
Fig. 7
K15-01
2500 m
Figs. 3, 5 & 6
b)
Wide deformation zone
Wide deformation zone
2500 m

Fig. 8

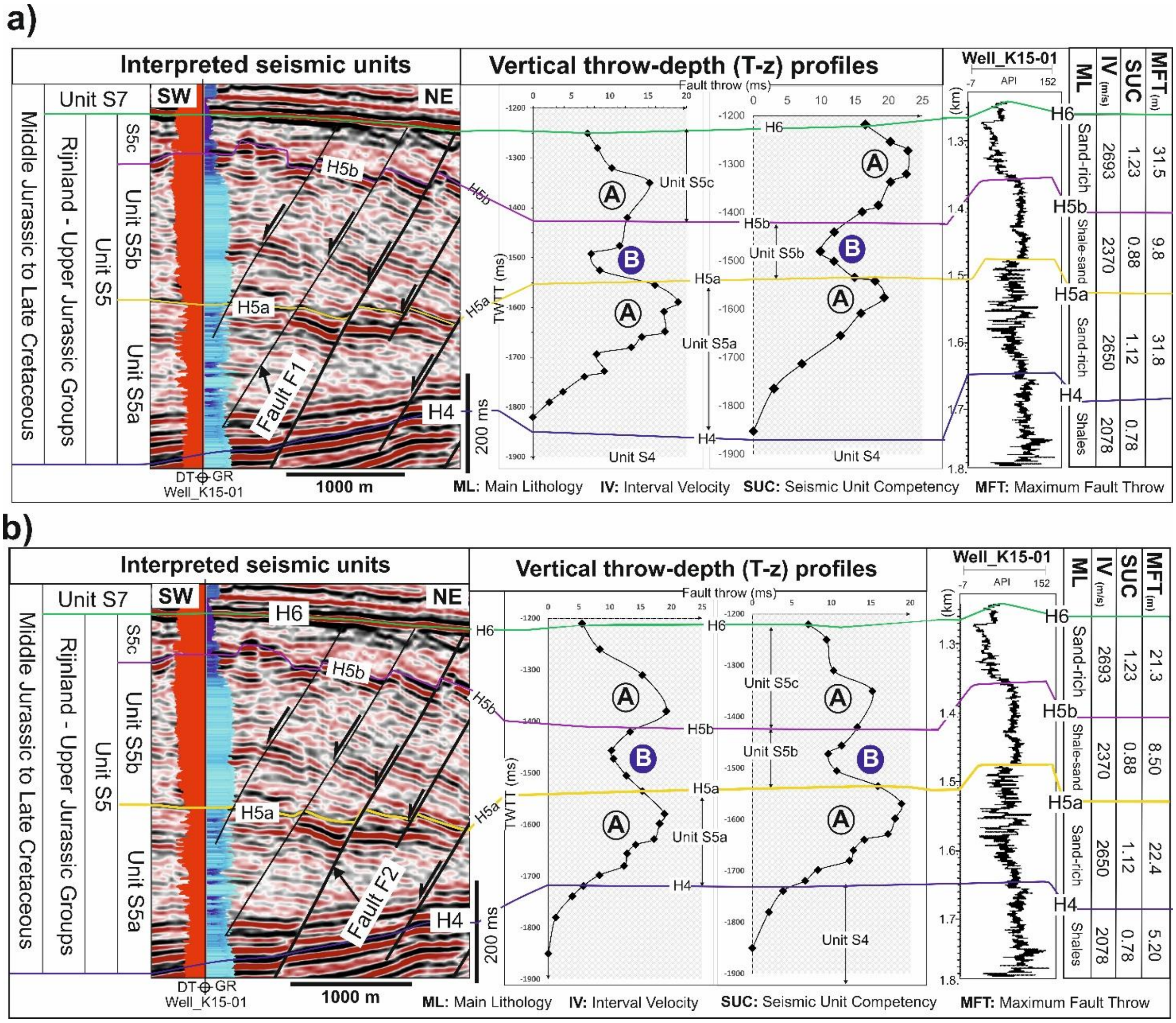
a)
Interpreted seismic units
Vertical throw-depth (T-z) profiles
Well_K15-01
ML
IV (m/s)
SUC
MFT (m)
Unit S7
Middle Jurassic to Late Cretaceous
Rijnland - Upper Jurassic Groups
Unit S5
S5c
Unit S5b
Unit S5a
SW
NE
H5b
H5a
H4
H6
Fault F1
200 ms
DT GR
Well_K15-01
1000 m
Fault throw (ms)
TWTT (ms)
Unit S5c
Unit S5b
Unit S5a
Unit S4
API
(km)
Sand-rich
Shale-sand
Shales
2693
2370
2650
2078
1.23
0.88
1.12
0.78
31.5
9.8
31.8
ML: Main Lithology
IV: Interval Velocity
SUC: Seismic Unit Competency
MFT: Maximum Fault Throw
b)
Interpreted seismic units
Vertical throw-depth (T-z) profiles
Well_K15-01
Fault F2
2693
2370
2650
2078
1.23
0.88
1.12
0.78
21.3
8.50
22.4
5.20
ML: Main Lithology
IV: Interval Velocity
SUC: Seismic Unit Competency
MFT: Maximum Fault Throw

Fig. 9

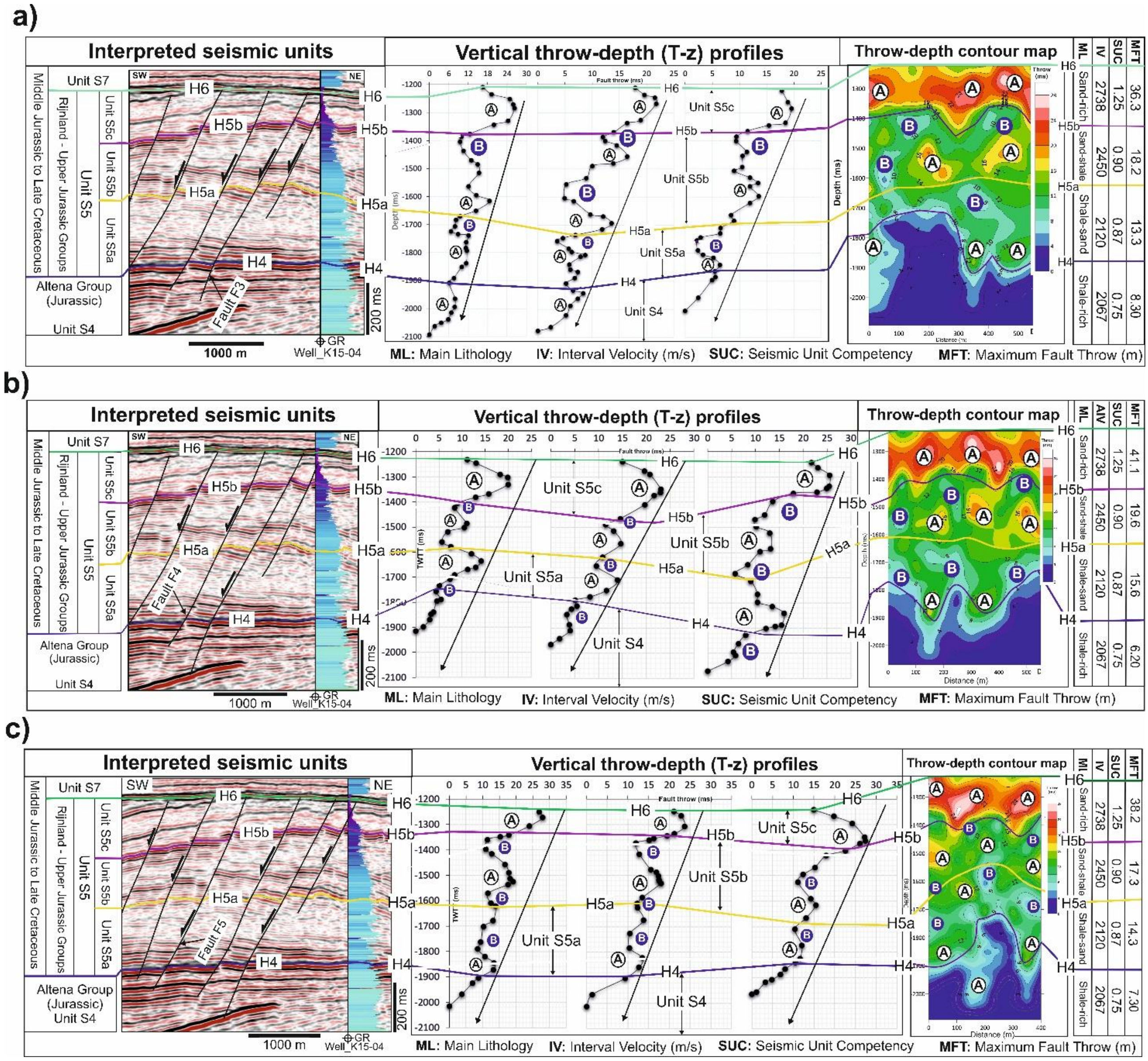

a)
Interpreted seismic units
Vertical throw-depth (T-z) profiles
Throw-depth contour map
ML
IV
SUC
MFT
Unit S7
Middle Jurassic to Late Cretaceous
Rijnland - Upper Jurassic Groups
Unit S5
Unit S5c
Unit S5b
Unit S5a
Altena Group (Jurassic)
Unit S4
H6
H5b
H5a
H4
Fault F3
1000 m
200 ms
Well_K15-04
Sand-rich
Sand-shale
Shale-sand
Shale-rich
2738
2450
2120
2067
1.25
0.90
0.87
0.75
36.3
18.2
13.3
8.30
ML: Main Lithology
IV: Interval Velocity (m/s)
SUC: Seismic Unit Competency
MFT: Maximum Fault Throw (m)
b)
Interpreted seismic units
Vertical throw-depth (T-z) profiles
Throw-depth contour map
AIV
Fault F4
41.1
19.6
15.6
6.20
c)
Interpreted seismic units
Vertical throw-depth (T-z) profiles
Throw-depth contour map
Fault F5
38.2
17.3
14.3
7.30

Fig. 10

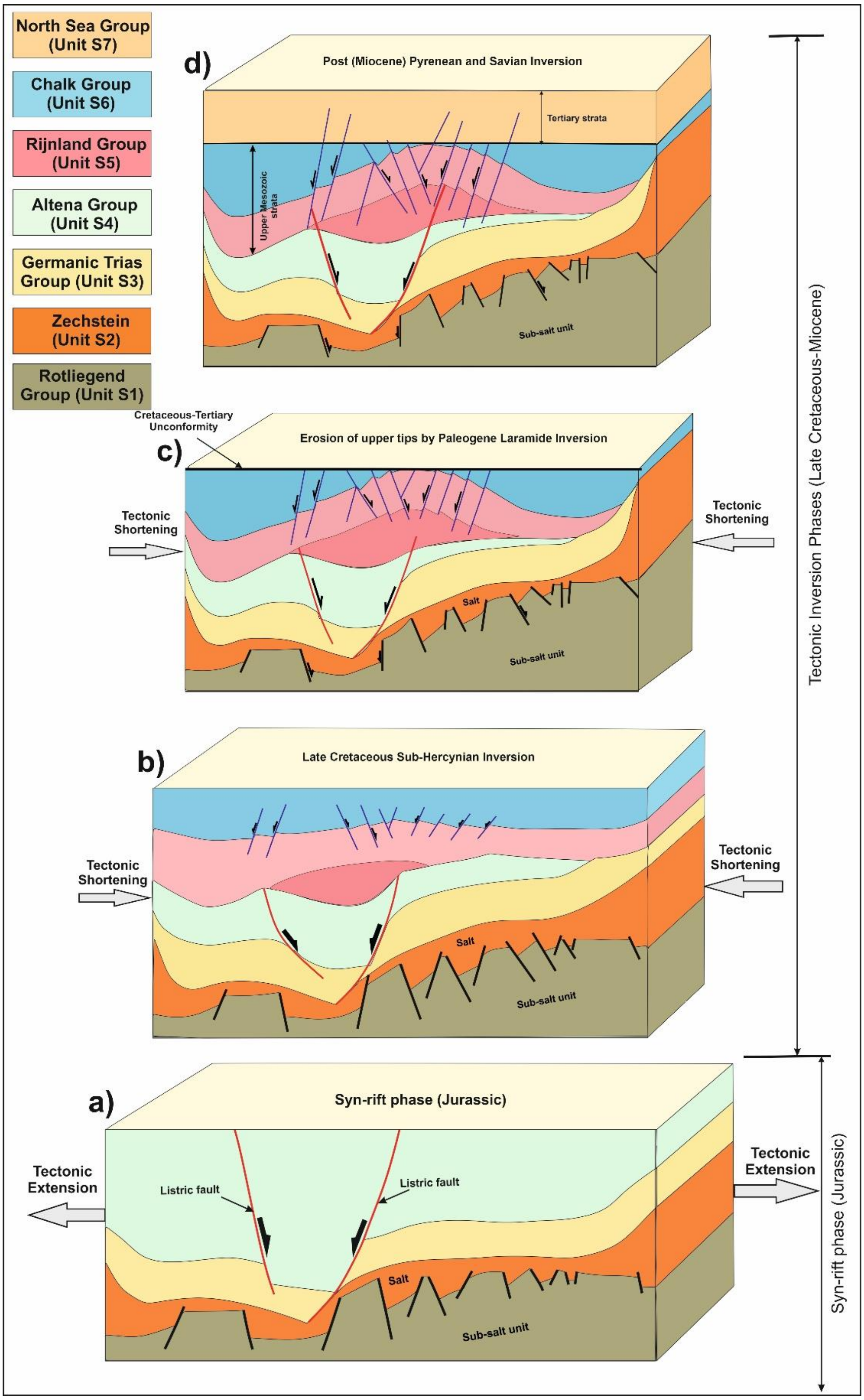
North Sea Group (Unit S7)
Chalk Group (Unit S6)
Rijnland Group (Unit S5)
Altena Group (Unit S4)
Germanic Trias Group (Unit S3)
Zechstein (Unit S2)
Rotliegend Group (Unit S1)
d)
Post (Miocene) Pyrenean and Savian Inversion
Tertiary strata
Upper Mesozoic strata
Sub-salt unit
Cretaceous-Tertiary Unconformity
c)
Erosion of upper tips by Paleogene Laramide Inversion
Tectonic Shortening
Tectonic Shortening
Salt
Sub-salt unit
b)
Late Cretaceous Sub-Hercynian Inversion
Tectonic Shortening
Tectonic Shortening
Salt
Sub-salt unit
a)
Syn-rift phase (Jurassic)
Tectonic Extension
Tectonic Extension
Listric fault
Listric fault
Salt
Sub-salt unit
Tectonic Inversion Phases (Late Cretaceous-Miocene)
Syn-rift phase (Jurassic)

Fig. 11

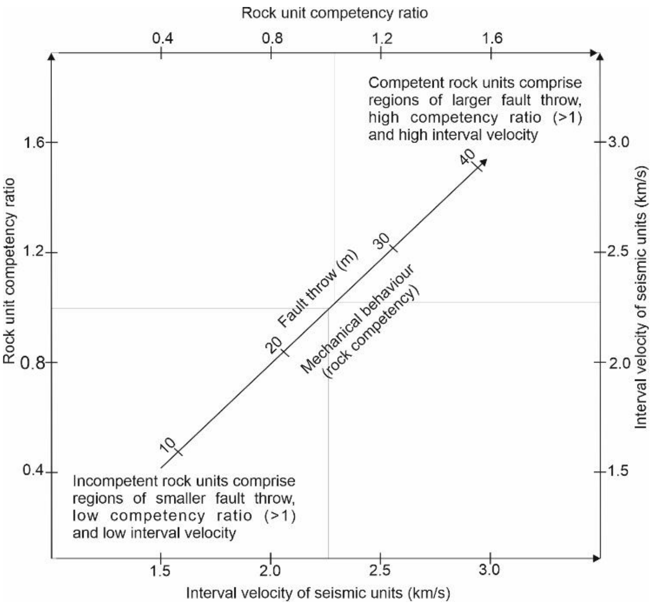
Rock unit competency ratio
0.4
0.8
1.2
1.6
Competent rock units comprise regions of larger fault throw, high competency ratio (>1) and high interval velocity
Rock unit competency ratio
1.6
1.2
0.8
0.4
Interval velocity of seismic units (km/s)
3.0
2.5
2.0
1.5
10
20
30
40
Fault throw (m)
Mechanical behaviour (rock competency)
Incompetent rock units comprise regions of smaller fault throw, low competency ratio (>1) and low interval velocity
1.5
2.0
2.5
3.0
Interval velocity of seismic units (km/s)

Fig. 12

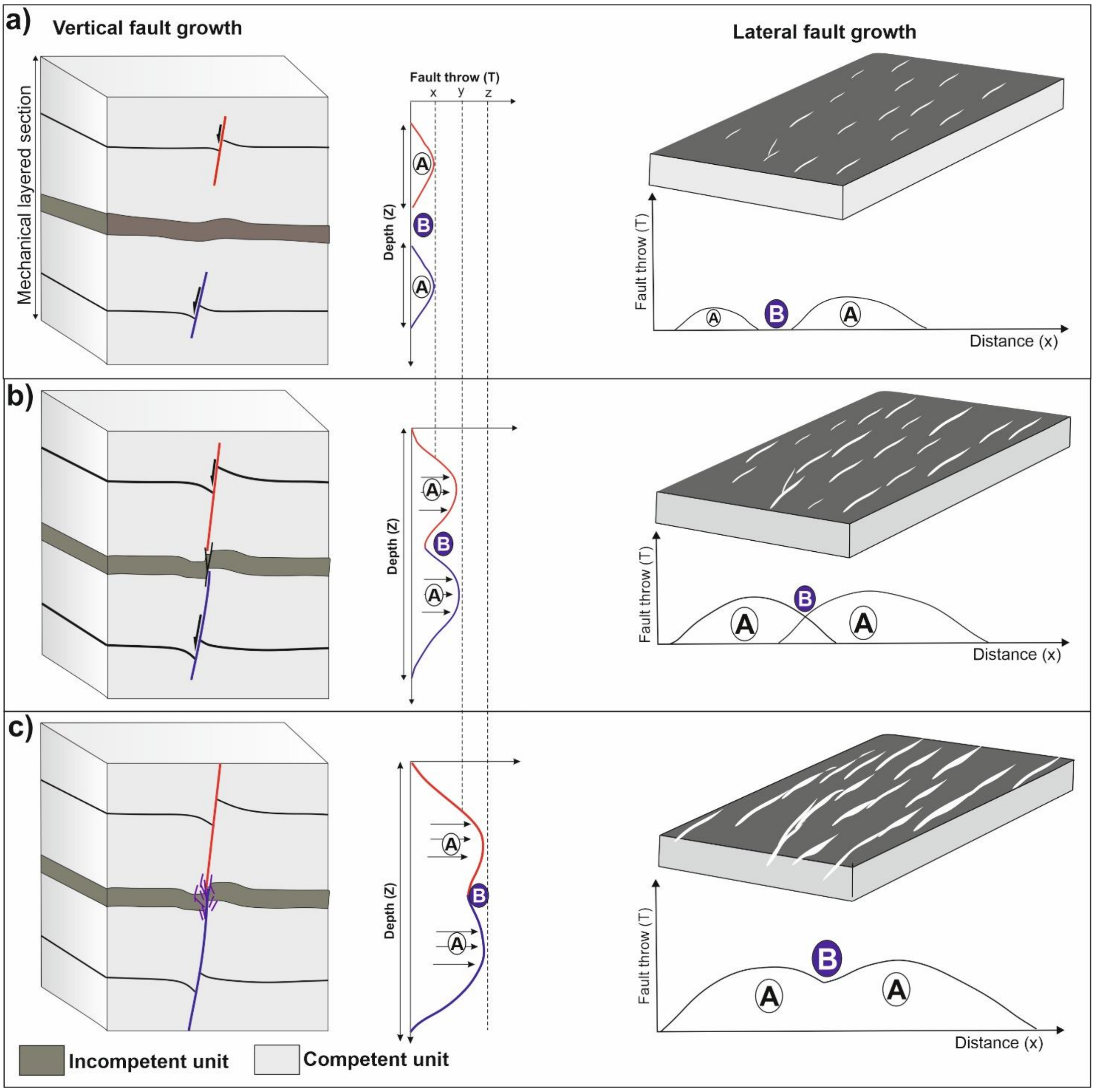
a)
Vertical fault growth
Lateral fault growth
Mechanical layered section
Fault throw (T)
x
y
z
Depth (Z)
A
B
Fault throw (T)
Distance (x)
b)
c)
Incompetent unit
Competent unit

Fig. 13

Table 1. Characteristics summary of the interpreted seismic units offshore Broad Fourteen Basin, Southern North Sea.

S/N	**Stratigraphic groups/age** (van Verweij and Simmelink. 2002)	**Tectonic Phase**	**Main lithologies** (Penge et al., 1999)	**Interpreted seismic units**	**Internal seismic features of the interpreted seismic units**	**Estimated thicknesses (m)**	**Interval velocities (m/s)**
1	North Sea Group (Paleocene to Recent)	Inversion Phase	Alternating sands, clays and shales.	Unit S7	High-frequency, moderate to high-amplitude and continuous seismic reflections characterised the seismic units. Densely spaced polygonal faults.	678	2185
2	Chalk Group (Late Cretaceous)		Limestones, marls, sands-calcareous	Unit S6	Chaotic internal reflections with low amplitude. The top of the unit (H6) generated a strong seismic reflector.	879	3907
3	Rijnland and Schieland Groups (Late Jurassic to Early Cretaceous)	Syn-rift Phase	claystones, some marls and sandstone beds.	Unit S5	Moderate to high-amplitude and high-frequency seismic reflections characterised the seismic unit. This seismic unit is locally deformed by faults and broad anticlines.	1035	2436
4	Altena Group (Late Triassic to Middle Jurassic)		Argillaceous deposits, Shales and calcareous sediments.	Unit S4	Characterised by a package of moderate to high amplitude, sparsely faulted reflectors and high-frequency seismic reflections.	517	2067
5	Germanic Trias Group (Early to Late Triassic)		Sandstones, carbonates, siltstones and claystones.	Unit S3	Moderate frequency and moderate to high-amplitude seismic reflections characterised the seismic unit.	618	2745
6	Zechstein Group (Late Permian)	Pre-rift and Rift onset Phase	Salt layers (Evaporites) and carbonate intervals.	Unit S2	Chaotic and low amplitude internal reflections forms the seismic unit.	840	4203
7	Rotliegend and Limburg Groups (Early to Middle Permian)		Sandstones, interbedded coal seams and coal measures.	Unit S1	Moderate frequency and faulted amplitude seismic reflections characterised the seismic unit.	1642	2856

Table 2. Characteristics summary of internal mechanical character of the interpreted seismic units S4, S5a, S5b and S5c.

S/N	**Seismic units**		**Well K15-01**							**Well K15-04**							
			Dominant lithology	Interval velocity (m/s)	Estimated thicknesses (m)	Competency ratio of the interpreted sub-seismic unit	Maximum fault throw (m)		Mechanical behaviour of seismic units	Dominant lithology	Interval velocity (m/s)	Estimated thicknesses (m)	Competency ratio of the interpreted sub-seismic unit	Maximum fault throw (m)			Mechanical behaviour of the seismic unit
							Fault F1	Fault F2						F3	F4	F5	
1	Unit S5	S5c	Sands-rich	2693	404	1.23	31.5	21.3	Competent	Sands-rich	2738	342	1.25	36.3	41.1	38.3	Competent
2		S5b	Shales-sands	2370	260	0.88	9.80	8.50	Incompetent	Sands-shales	2450	270	0.90	18.2	19.6	17.3	Incompetent
3		S5a	Sands-rich	2650	371	1.12	31.8	22.4	Competent	Shales-sands	2120	212	0.87	13.3	15.6	14.3	Incompetent
4	Unit S4		Shales-rich	2078	528	0.78		5.20	Incompetent	Shales-rich	2067	517	0.75	8.30	6.20	7.30	Incompetent